Research Square

Preprints are preliminary reports that have not undergone peer review.
They should not be considered conclusive, used to inform clinical practice,
or referenced by the media as validated information.

A Probiotic Formula Reshapes Oral-Gut Microbiota, Attenuates the Gut Resistome, and Supports Lean Growth in Preschoolers: A Multi-Omics Trial

Meng Zhang
Key Laboratory of Dairy Biotechnology and Engineering, Ministry of Education, Inner Mongolia Agricultural University, Hohhot 010018, China.

Xin Han
Key Laboratory of Dairy Biotechnology and Engineering, Ministry of Education, Inner Mongolia Agricultural University, Hohhot 010018, China.

Zhengdong Liu
Inner Mongolia Mengniu Dairy (Group) Limited by Share Ltd. Hohhot 011500, China.

Kaiyang Liu
Key Laboratory of Dairy Biotechnology and Engineering, Ministry of Education, Inner Mongolia Agricultural University, Hohhot 010018, China.

Xuezhen Zhou
Inner Mongolia Mengniu Dairy (Group) Limited by Share Ltd. Hohhot 011500, China.

Xingwang Ye
Inner Mongolia Mengniu Dairy (Group) Limited by Share Ltd. Hohhot 011500, China.

Zhenyu Yang
National Institute for Nutrition and Health, Chinese Center for Disease Control and Prevention/Key Laboratory of Human Milk Science, Chinese Center for Disease Control and Prevention/NHC Key Laboratory of Public Nutrition and Health, Beijing 100050, China.

Yanmei Ma
National Institute for Nutrition and Health, Chinese Center for Disease Control and Prevention/Key Laboratory of Human Milk Science, Chinese Center for Disease Control and Prevention/NHC Key Laboratory of Public Nutrition and Health, Beijing 100050, China.

Lai-Yu Kwok
Key Laboratory of Dairy Biotechnology and Engineering, Ministry of Education, Inner Mongolia Agricultural University, Hohhot 010018, China.

Yifan Duan
National Institute for Nutrition and Health, Chinese Center for Disease Control and Prevention/Key Laboratory of Human Milk Science, Chinese Center for Disease Control and Prevention/NHC Key Laboratory of Public Nutrition and Health, Beijing 100050, China.

Wenyi Zhang

zhangwenyizi@163.com

Key Laboratory of Dairy Biotechnology and Engineering, Ministry of Education, Inner Mongolia Agricultural University, Hohhot 010018, China.

Heping Zhang

Key Laboratory of Dairy Biotechnology and Engineering, Ministry of Education, Inner Mongolia Agricultural University, Hohhot 010018, China.

Research Article

Keywords: Antibiotic resistance, Bifidobacterium animalis subsp. lactis, Body composition, Lean growth, Microbial coupling, Multi-omics

Posted Date: April 29th, 2026

DOI: https://doi.org/10.21203/rs.3.rs-9483549/v2

License: This work is licensed under a Creative Commons Attribution 4.0 International License. Read Full License

Additional Declarations: The authors declare potential competing interests as follows: Zhengdong Liu, Xuezhen Zhou, and Xingwang Ye are affiliated with Inner Mongolia Mengniu Dairy (Group) Limited by Share Ltd. The remaining authors declare no competing financial or commercial interests.

A Probiotic Formula Reshapes Oral-Gut Microbiota, Attenuates the Gut Resistome, and Supports Lean Growth in Preschoolers: A Multi-Omics Trial

Meng Zhang[1,2,3,§], Xin Han[1,2,3,§], Zhengdong Liu[4,§], Kaiyang Liu[1,2,3], Xuezhen Zhou[4], Xingwang Ye[4], Zhenyu Yang[5], Yanmei Ma[5], Lai-Yu Kwok[1,2,3], Yifan Duan[5,#], Wenyi Zhang[1,2,3,#], Heping Zhang[1,2,3,#]

[1]Key Laboratory of Dairy Biotechnology and Engineering, Ministry of Education, Inner Mongolia Agricultural University, Hohhot 010018, China.

[2]Key Laboratory of Dairy Products Processing, Ministry of Agriculture and Rural Affairs, Inner Mongolia Agricultural University, Hohhot 010018, China.

[3]Inner Mongolia Key Laboratory of Dairy Biotechnology and Engineering, Inner Mongolia Agricultural University, Hohhot 010018, China.

[4]Inner Mongolia Mengniu Dairy (Group) Limited by Share Ltd. Hohhot 011500, China.

[5]National Institute for Nutrition and Health, Chinese Center for Disease Control and Prevention/Key Laboratory of Human Milk Science, Chinese Center for Disease Control and Prevention/NHC Key Laboratory of Public Nutrition and Health, Beijing 100050, China.

[§]Equal contribution

[#]Correspondence to: Heping Zhang (hepingdd@vip.sina.com), Wenyi Zhang (zhangwenyizi@163.com), and Yifan Duan (duanyf@ninh.chinacdc.cn)

Abstract

The preschool years represent a modifiable window for shaping growth and microbiome development. In a two-month cluster randomized trial of 317 Chinese kindergarten children, we evaluated a formula enriched with *Bifidobacterium animalis* subsp. *lactis* Probio-M8. The intervention promoted greater gains in height and fat-free mass without increasing body mass index. Multi-omics profiling (saliva 2bRAD-M, fecal metagenomics, metabolomics) revealed site-specific microbiome remodeling, reduced oral-gut microbial coupling, and a net contraction of the gut resistome, particularly in efflux-associated genes. The fecal metabolome showed a biphasic response: early shifts in energy metabolism gave way to later enrichment of lipid mediators (e.g., resolvin D2) and neuroactive compounds. Integrative networks linked *Bifidobacterium*-enriched communities and metabolite signatures to improved growth and lower antibiotic use. These findings demonstrate that probiotic nutrition during preschool can coordinately enhance lean growth, refine microbiome organization, and reduce antimicrobial resistance potential in real-world settings.

Keywords: Antibiotic resistance; *Bifidobacterium animalis* subsp. *lactis*; Body composition; Lean growth; Microbial coupling; Multi-omics

Introduction

Early life is widely recognized as a critical window during which host immunity and the microbiome co mature.[1,2] Yet the preschool period is often treated as a mere "readout" of earlier developmental trajectories, rather than as a tractable stage for intervention.[3,4] This view overlooks a defining ecological and clinical transition. Upon entry into group settings, children experience sharply increased close contact and pathogen exposure; respiratory illnesses become common, and antibiotic use is far from rare.[5-7] Meanwhile, mucosal immunity, epithelial barrier function, and metabolic homeostasis continue to mature and remain plastic.[8,9] Thus, the preschool years represent not only a readout of prior development but also a vulnerable and modifiable phase, one in which scalable nutritional strategies could plausibly improve growth trajectories while simultaneously reducing infection-related medical burden under real world conditions.[10,11]

A growing body of evidence positions the gut microbiome as a key integrator of diet and host phenotypes relevant to child health, including nutrient harvest, metabolic signaling, barrier maintenance, and immune education.[1,12,13] Perturbations during childhood, whether driven by infections, antibiotic exposures, or environmental shifts,[14,15] can propagate through the gut ecosystem and feed back onto host susceptibility and development.[16,17] However, demonstrating how a feasible nutritional intervention reshapes the microbiome and metabolome system over time,[18] and how these changes align with clinically meaningful outcomes, remains challenging. Longitudinal, multi-layer profiling is particularly important in preschool cohorts, where both exposures and biological responses can change rapidly across weeks and months.[19]

Beyond the gut, the oral cavity is one of the most densely colonized microbial habitats and is closely connected to the upper respiratory tract and mucosal immune tone.[20,21] Oral microbes and their products continuously enter the gastrointestinal tract via swallowing and mucosal trafficking, fueling interest in an oral-gut microbial axis.[22,23] From an ecological perspective, increased cross-site similarity, such as synchronized fluctuations in shared taxa, may reflect reduced niche specialization and greater microbial dispersal across body sites. Conversely, lower cross-site sharing and weaker coupling are typically associated with site-specific differentiation and compartmentalization.[23-28] Despite the relevance of these concepts, longitudinal evidence in preschool children remains limited, and it is unclear whether nutrition-based interventions can modulate oral-gut coupling in parallel with health-related endpoints.

Antibiotic exposure intersects with these dynamics through its effects on the childhood resistome.[29] Antibiotic use and transmission within group environments may promote the accumulation and persistence of antibiotic resistance genes (ARGs), making the resistome a useful indicator of selective pressure and potential antimicrobial risk.[29,30] Nutrition-centered microbiome interventions have been proposed as a strategy to reduce resistome burden, through mechanisms such as ecological replacement, competitive exclusion, and functional shifts, without imposing additional antimicrobial pressure.[31,32] Yet evidence in healthy preschool populations remains sparse, particularly for studies that track resistome trajectories longitudinally, profile both oral and gut microbiomes, and interpret resistome changes alongside illness and medication outcomes within a unified trial framework.

Probiotics, defined as live microorganisms that confer a health benefit when administered in adequate amounts, offer a practical route to scalable interventions.[33] Bifidobacteria are important members of the human gut ecosystem, frequently associated with carbohydrate utilization, microbial cross-feeding, and host-microbe communication.[34] *Bifidobacterium animalis* subsp. *lactis* Probio-

M8 (Probio-M8) has shown potential in prior work for modulating microbiota features and immune related readouts,[35,36] and probiotic-enriched formulas are increasingly used in children.[37-39] Nevertheless, key gaps remain: many studies focus exclusively on the gut, fail to capture coordinated oral ecosystem dynamics, and rarely resolve time-dependent patterns that distinguish early responses from later stabilization.

Here, we conducted a two-month cluster randomized controlled trial in 5- to 6-year-old preschool children to evaluate a Probio-M8 enriched formula in a kindergarten setting. We assessed growth and body composition, respiratory illness incidence, and antibiotic use, and profiled the oral microbiome using 2bRAD-M, the gut metagenome and resistome via shotgun metagenomics, and the fecal metabolome using untargeted metabolomics at baseline, two weeks, and two months. This design allowed us to examine whether Probio-M8 formula intake was associated with favorable developmental outcomes, shifts in oral and gut microbial community patterns, including altered cross-site coupling, and temporal changes in the gut resistome and fecal metabolome. By integrating clinical endpoints with multi-omics measurements across oral and gut compartments, our study provides a trial-based view on how probiotic nutrition relates to microbiome organization and antimicrobial resistance potential during a vulnerable yet actionable phase of early childhood.

Results

Growth-related outcomes from this preschool cohort have been partially reported previously in a peer-reviewed Chinese-language journal.[40] Here, we summarize only key anthropometric endpoints as clinical readouts and focus primarily on the added multi-omics layers, including paired oral and gut microbiome profiling, gut resistome characterization, and fecal metabolomics, alongside integrative analyses linking these features to growth and infection related phenotypes.

Cohort characteristics and clinical outcomes during the trial

A total of 373 children were assessed for eligibility, 320 entered cluster allocation, and 317 completed follow-up (**Fig. 1a**, **Fig. S1**). For clinical phenotype analyses, 301 participants with complete metadata and anthropometric records were included (intervention group, receiving Probio-M8 formula, n = 167; control group, n = 134). Baseline characteristics were broadly comparable between groups, including sex, delivery mode, feeding history, and baseline height, weight, body mass index (BMI), and fat free mass (FFM; $P > 0.05$; **Table 1**). The intervention group was slightly older on average, though the absolute difference was small over the two-month observation window ($P < 0.05$; **Table 1**). Stool consistency also differed at baseline, with a higher proportion of abnormal stool form in the control group (**Table 1**); this difference diminished during follow-up.

Over the two-month period, both groups exhibited increases in height and weight, but the magnitude of change was larger in the intervention group ($P < 0.05$; **Fig. 1b**). Specifically, the intervention group showed a significantly greater increase in height ($P < 0.05$; **Fig. 1c**) and a modestly greater increase in weight ($P < 0.05$). Body mass index did not differ between groups at any time point, and changes in BMI were not significantly different ($P > 0.05$; **Fig. 1b**). Fat free mass increased in both groups, with a larger gain in the intervention group ($P < 0.05$; **Fig. 1b**). Collectively, these data indicate that Probio-M8 formula intake was associated with enhanced linear growth and greater accrual of lean mass over two months, without a measurable increase in BMI at the group level.

At baseline, abnormal stool form was more common in the control group than in the

intervention group (17% vs. 8%, $P < 0.05$; **Table 1**). During follow up, stool form in both groups shifted toward a healthier profile, with the proportion of children reporting healthy stool exceeding 85% at both the 2-week and 2-month time points; no clear between-group differences were observed at these later visits.

Respiratory illness incidence fluctuated modestly over time, but group differences did not reach statistical significance at individual time points, nor were overall trends detectably different ($P > 0.05$; **Table 1**). Antibiotic use was higher in the control group at baseline and at two weeks (baseline: 14% vs. 3%, $P < 0.05$; two weeks: 11% vs. 6%, $P < 0.05$), though this difference attenuated by two months (19% vs. 13%, $P > 0.05$; **Table 1**). For allergic outcomes, most comparisons were non-significant, with the exception of allergic rhinitis at two weeks, which was less frequent in the intervention group ($P < 0.05$; **Table 1**).

Taken together, within the two-month intervention window, Probio-M8 formula intake was characterized by three main patterns: (1) Greater gains in height and FFM, despite broadly comparable baseline profiles, without a detectable increase in BMI at the group level; (2) A lower frequency of antibiotic use during the early follow-up period in a kindergarten setting marked by high exposure to respiratory pathogens; and (3) Improvement in gastrointestinal function over time in both groups, with symptom profiles converging to similar levels by the end of follow-up.

Probio-M8 formula remodels oral and gut community structure in distinct directions and reduces oral-gut coupling

To investigate microbiome-level changes, we established a paired oral and gut multi-omics dataset from participants with at least one available time point sample. This included salivary microbial profiling by 2bRAD-M (913 samples from 310 participants), fecal shotgun metagenomics (886 samples from 310 participants), and fecal untargeted metabolomics (887 samples from 311 participants) collected at baseline, week 2, and month 2 (**Fig. 1a**, **Fig. S1**).

Across the cohort, only a small fraction of microbial taxa was detected in both saliva and stool. This shared taxonomic set accounted for approximately 3-4% of total oral microbial abundance and about 2% of total gut microbial abundance, with proportions remaining relatively stable across time points and study groups (**Fig. 2a**). To quantify within-individual coordination between oral and gut communities, we computed two metrics, L2 similarity and Spearman correlation, based on the abundances of these shared taxa (**Fig. 2a, b**). In the intervention group, oral-gut similarity decreased progressively over time, with month 2 values significantly lower than those at baseline and week 2 ($P < 0.05$; **Fig. 2b**). Cross-site concordance followed a parallel decline. In contrast, both coupling metrics remained stable in the control group ($P > 0.05$). Together, these results indicate that Probio-M8 formula intake was associated with a time-dependent reduction in coupling between shared oral and gut taxa, evident in both compositional similarity and coordinated abundance dynamics.

At the diversity level, Probio-M8 induced divergent effects across body sites (**Fig. 2c**, **Fig. S2a**). Oral alpha diversity decreased after intervention initiation and remained significantly lower than in controls at both week 2 and month 2 (Shannon and Simpson indices, $P < 0.05$). Conversely, gut alpha diversity showed a transient increase at week 2, returning toward control levels by month 2 ($P < 0.05$; **Fig. 2c**). Functional alpha diversity (derived from CAZy and KEGG annotations) showed less pronounced shifts, with only selective time point-specific differences ($P < 0.05$; **Fig. S2a**), suggesting that the intervention primarily reshaped the relative weighting of specific microbial functions rather than broadly expanding or compressing total functional repertoire.

We next used permutational multivariate analysis of variance (PERMANOVA) to assess factors driving variation in microbial and functional profiles (**Fig. 2d**). Both treatment group and time point emerged as major contributors across the oral microbiome, gut microbiome, and multiple functional layers, including ARG profiles, CAZy families, and KEGG modules (F_{sum} = 40.530 and 27.420, respectively). Several host and environmental covariates, including sex and respiratory illness status, also contributed significantly to variation in selected data layers (F_{sum} = 22.705, 21.545, and 18.246; **Fig. 2d**).

Bray-Curtis-based ordination further revealed site-specific trajectories. The oral microbiome showed group separation as early as baseline, which persisted throughout follow-up (PERMANOVA: baseline, F = 3.655, P = 0.001; week 2, F = 5.386, P = 0.001; month2, F = 2.444, P = 0.004; **Fig. 2e**). In contrast, the gut microbiome showed no detectable group difference at baseline (F = 1.002, P=0.418) but became clearly separated at week 2 (F = 2.983, P = 0.001) and remained separated at month 2 (F = 2.991, P = 0.002; **Fig. 2e**, **Fig. S2b**). Similarly, ordinations of ARG profiles, CAZy families, KEGG and KEGG pathways revealed structured, time-dependent shifts and consistent group separation (**Fig. 2f**, **Fig. S2b**). In alignment with these community-level patterns, the total number of annotated ARGs in the intervention group showed a progressive decline, reaching levels significantly lower than baseline by month 2 and significantly below those of the control group at that time point (P < 0.05; **Fig. S2c**).

Species-level changes highlight oral streptococci remodeling and bifidobacteria enrichment in stool

To characterize community-level remodeling associated with Probio-M8 formula, we performed species-level differential abundance analyses on saliva and fecal metagenomes, excluding taxa that changed in the same direction across all time points, thereby filtering out features more likely to reflect stable baseline differences rather than intervention effects. This approach yielded 55 intervention-associated species, comprising 38 oral and 17 gut taxa (**Fig. 3a**). Overall, Probio-M8 formula was linked to a dual-pattern shift: a subset of inflammation-associated oral microbes decreased in saliva, while bifidobacteria and other potentially immunoregulatory commensals gained ecological prominence in stool, resulting in two niche-specific, yet directionally concordant, core communities.

In the oral cavity, the control group exhibited relative stability in microbial composition from baseline to month 2, whereas the Probio-M8 formula group showed pronounced shifts after intervention (Fig. 3a). Among core species, *Mogibacterium diversum*, *Porphyromonas* sp003640335, and *Rothia mucilaginosa* showed no significant intergroup differences at baseline but were consistently and significantly depleted in the intervention group at both week 2 and month 2 (P < 0.05; **Fig. 3b**).

A second set of streptococci displayed an opposite temporal pattern. *Streptococcus (S.) oralis*, *S. parasanguinis*, and *S. pseudopneumoniae* were slightly more abundant in the Probio-M8 group at baseline, potentially indicating an initial imbalance, but by week 2 and month 2, all three species were significantly less abundant than in controls (P < 0.05; **Fig. 3b**). These streptococci are known to participate in early tooth surface colonization and dental plaque maturation and have been implicated in oral immune tolerance and tissue repair processes.[41-43] Their transient enrichment at baseline, followed by a coordinated decline alongside other putative cariogenic or inflammation-associated taxa, is consistent with the hypothesis that Probio-M8 formula drives oral community

reorganization toward a configuration in which health-associated commensal streptococci assume a more central ecological role.

In the gut, Probio-M8 formula strengthened the ecological prominence of bifidobacteria and selected co-occurring commensals (**Fig. 3a, b**). *Bifidobacterium (B.)* was significantly enriched at both week 2 and month 2 ($P < 0.05$), indicating sustained colonization over the two-month intervention period in this preschool cohort. In contrast, *Bacteroides (Ba). stercoris* exhibited a more complex trajectory, with evidence of an overall decline by month 2. Previous work has linked *Ba. stercoris* to adverse outcomes such as inflammatory bowel disease and autism spectrum disorders,[44-46] although certain strains have also been associated with anti-obesity effects,[47,48] underscoring its context-dependent functionality. In our study, the systematic reduction of *Ba. stercoris* is more plausibly interpreted as a rebalancing of strain-level or functional subgroups within the species, rather than a uniformly beneficial or detrimental shift.

Probio-M8 formula also selectively reduced several taxa previously associated with inflammation or ectopic colonization (**Fig. 3a, b**). *Eisenbergiella tayi* and *Megasphaera micronuciformis* did not differ significantly between groups at baseline or week 2 but were markedly lower in the intervention group by month 2 ($P < 0.05$). *Eisenbergiella tayi* has been proposed to degrade mucin and potentially compromise epithelial barrier integrity, with emerging links to neuroimmune conditions,[49] while *Megasphaera micronuciformis* is frequently reported in studies of oral dysbiosis.[50,51] The detection of these taxa in fecal samples may thus reflect a risk-associated signature, potentially originating from oral or external sources. Their sustained decline following Probio-M8 intake aligns with our earlier observations of reduced oral-to-gut microbial coupling and decreased contribution of orally derived taxa to the gut community.

At the functional level, differential features in CAZy families, KEGG modules and pathways exhibited marked temporal structure (**Fig. S3a, b**). Most functional differences emerged only after intervention initiation, with minimal differences at baseline. Venn diagram analyses showed that only a small fraction of functional features were consistently altered across all three time points; instead, month 2-specific differences predominated (**Fig. S3b**). These observations suggest that Probio-M8 formula does not merely amplify preexisting metabolic capacities. Rather, it is associated with the progressive acquisition of new combinations of carbohydrate-active enzymes and metabolic pathways in both oral and gut microbiomes, providing a functional substrate that may underpin subsequent improvements in metabolic homeostasis.

Probio-M8 formula is associated with contraction of the gut resistome and shifts in resistance mechanism composition

Given the observed patterns of antibiotic use and structured functional shifts in the gut microbiome, we examined the gut resistome using PathoFact annotations of fecal metagenomes. Across the cohort, ARGs spanned multiple resistance mechanisms, including efflux, target modification, enzymatic inactivation, and altered membrane permeability (**Fig. S4**).

Differential abundance analysis identified 29 ARGs that were consistently lower in the intervention group compared to controls at both week 2 and month 2 (**Fig. 3c**). This decreased set was enriched for multidrug efflux-related components, including *acrB*, *baeS*, *emrD*, *emrR*, *macA*, *marA*, and *ompF*, as well as genes associated with resistance to cell wall-targeting antibiotics, such as *pbp_1B* (**Fig. 3c**). Only a small number of ARGs persistently increased across both follow-up time points.

Time-stratified comparisons suggested that the magnitude and breadth of ARG reductions were most prominent at week 2. By month 2, the total number of significantly decreased ARGs had diminished, but a core subset remained consistently suppressed (**Fig. 3c**). Aggregation of ARGs by resistance mechanism showed an overall decrease in the total abundance of several major categories at week 2, with efflux-related mechanisms exhibiting the largest reductions. At month 2, these categories remained lower on average, although some heterogeneity within individual mechanisms was evident (**Fig. 3d**, **Fig. S4**).

Collectively, these findings indicate that Probio-M8 formula intake was associated with a net contraction of the gut resistome and a progressive reweighting of its functional composition, suggesting a potential role for probiotic nutrition in mitigating antimicrobial resistance burden during early childhood.

Probio-M8 elicits biphasic remodeling of the fecal metabolome: from early energy-immune activation to late lipid-neuroimmune signaling

To examine how Probio-M8 formula influences metabolic adaptation at the gut level, we performed untargeted LC-MS-based metabolomics on fecal samples and annotated over 1,200 metabolites. We compared metabolite abundances and pathway enrichment between the Probio-M8 and control groups at baseline, week 2, and month 2 (**Fig. 4**). Distinct sets of discriminatory metabolites emerged at each time point, revealing a clear temporal evolution in the metabolic response (**Fig. 4a, b**). At baseline, a modest number of differential metabolites were observed, likely reflecting preexisting differences in habitual diet, lifestyle, or health status. By week 2, the number of significantly differential metabolites peaked, indicating a broad and directionally coherent metabolic perturbation. At month 2, the total number of differential metabolites decreased, but their composition shifted toward lipid-derived and neuroactive compounds. Intersection and union analyses across time points identified 76 metabolites that changed consistently in the same direction throughout the intervention period (**Fig. 4c**); this core set was designated the metabolic signature of Probio-M8 intake.

During the early intervention phase (week 2), differential metabolites were concentrated in pathways related to energy metabolism, amino acid turnover, and mucosal immune regulation (**Fig. 4d**). Multiple intermediates of the tricarboxylic acid cycle and central carbon metabolism, including citrate, isocitrate, fumarate, and malate, were significantly altered, alongside amino acids such as glutamine, arginine, alanine, aspartate, and their derivatives. Corresponding pathways, including alanine, aspartate, and glutamate metabolism; arginine biosynthesis; arginine and proline metabolism; and the citrate cycle, were all significantly enriched. These findings suggest a rapid recalibration of basal energy and nitrogen metabolism through host-microbe co-metabolism in response to Probio-M8.

Concurrently, pathways linked to mucosal immunity, specifically the intestinal immune network for "IgA production" and "*Staphylococcus aureus* infection", were enriched. Chemotactic peptides and small peptide-like molecules occupied central positions in the co-occurrence network connecting metabolic and immune nodes, implying active reorganization of mucosal barrier function. Notably, dopamine and its precursors contributed to enrichment of dopaminergic synapse and related signaling pathways, indicating early engagement of catecholamine metabolism along the gut-brain axis. Collectively, the week 2 metabolomic profile reflects a coordinated activation of central energy metabolism alongside innate and mucosal immune processes.

By month 2, the metabolic landscape transitioned from broad perturbation to selective remodeling of lipid and neuroimmune signaling networks (**Fig. 4d**). Pathway enrichment analyses highlighted linoleic acid metabolism, steroid hormone biosynthesis, neuroactive ligand-receptor interaction, cAMP signaling, and cGMP-PKG signaling. Several unsaturated fatty acids and their oxidized derivatives, including 9-oxoODE, 13*S*-HODE, and 9,10,13-TriHOME, were persistently elevated in the intervention group, signaling a systematic reshaping of the intestinal lipid mediator profile. Cholesterol, aldosterone, and their precursors contributed to steroid hormone pathway enrichment, suggesting modulation of endocrine regulatory axes. Critically, the specialized pro-resolving mediator, resolvin D2, and multiple neuroactive molecules, including GABA, histamine, norepinephrine, and aromatic amines, were significantly elevated in the intervention group. In combination with enrichment of the neuroactive ligand receptor interaction and Th17 cell differentiation pathways, these changes point to a rebalancing of gut-neuro-immune crosstalk.

Together, the month 2 metabolomic profile is consistent with a state of refined homeostatic regulation, dominated by lipid mediators and neuroimmune signaling, rather than an acute inflammatory or metabolic stress response.

Multi-omics association analyses indicate that Probio-M8 formula reshapes microbe-metabolite-phenotype connectivity

To further explore how Probio-M8 formula relates to growth promotion, reduced antibiotic use, and lower respiratory illness burden, we constructed a series of correlation networks centered on intervention-associated metabolites. Using differentially abundant metabolites as anchors, we first built metabolite-phenotype and metabolite-species Spearman correlation networks (**Fig. 5a, b**), then integrated these layers into a unified multi-omics co-occurrence network for the intervention and control groups (**Fig. 5c**).

In the metabolite-phenotype network (**Fig. 5a**), height and FFM clustered together, forming a distinct growth-related module. Metabolites such as N^2-gamma-glutamylglutamine, pymetrozine, and xanthoxylin showed positive correlations with height and/or FFM, whereas digitogenin, asiatic acid, deoxycorticosterone acetate, sinapic acid, ketoleucine, and several structurally related compounds correlated negatively with these traits. Given the observed intervention effects, this pattern suggests that higher levels of selected amino acid and peptide-like metabolites coincide with more favorable linear growth and lean mass accretion during Probio-M8 formula intake, while a subset of steroid-like and aromatic acid metabolites tends to be enriched in children with comparatively lower height and FFM.

Antibiotic use and respiratory illness coalesced into a second module reflecting infection and medication burden (**Fig. 5a**). Metabolites including 5-oxo-1,2-campholide, (*R*)-mandelic acid, deoxyinosine, 1-hexadecanol, 2,3-butanediol, and 5α-cholest-8-en-3β-ol showed positive correlations with antibiotic use; notably, 5-oxo-1,2-campholide and (*R*)-mandelic acid were also positively correlated with respiratory illness. In contrast, glycyrrhetinic acid, gabapentin, 3-ketosphingosine, and theophylline were negatively correlated with antibiotic use, and gabapentin further exhibited a negative association with respiratory illness. In light of the lower rates of antibiotic use and respiratory illness observed in the Probio-M8 formula group, these findings suggest that metabolite signatures linked to higher treatment and infection burden, such as 5-oxo-1,2-campholide, (*R*)-mandelic acid, deoxyinosine, and 2,3-butanediol, were down-weighted during the intervention, whereas metabolites associated with reduced medication and infection burden,

such as glycyrrhetinic acid, gabapentin, 3-ketosphingosine, and theophylline, were relatively more prominent.

In the metabolite-microbiota correlation layer (**Fig. 5b**), *B. animalis* and *Ba. stercoris*, both of which increased in relative abundance with Probio-M8 formula intake, participated in multiple significant associations. These two species were more frequently positively correlated with metabolites that themselves associated positively with height and FFM (e.g., N^2-gamma-glutamylglutamine, pymetrozine, xanthoxylin) and less often positively correlated with metabolites tracking with antibiotic use or respiratory illness (e.g., 5-oxo-1,2-campholide, (*R*)-mandelic acid, deoxyinosine, 2,3-butanediol). Conversely, taxa enriched in the control group or linked to less favorable clinical outcomes more commonly connected to metabolite nodes positively associated with antibiotic use and respiratory illness. Although these analyses are correlational and cannot establish causality or directionality, they support a model in which higher abundances of *B. animalis*, *Ba. stercoris*, and related taxa co-occur with metabolite profiles linked to better growth and reduced treatment burden, while risk-associated metabolite-phenotype patterns are attenuated.

When differential species and metabolites were integrated into a single multi-omics network (**Fig. 5c**), the intervention and control groups showed consistent differences in global topology. The intervention network contained more nodes and edges than the control network (nodes: 292 vs. 280; edges: 12,393 vs. 9,746), with a higher mean number of neighbors (87.541 vs. 70.609). Network density (0.310 vs. 0.257) and clustering coefficient (0.765 vs. 0.666) were also greater in the intervention group, while characteristic path length (2.169 vs. 2.586) and network diameter (8 vs. 9) were reduced. Network heterogeneity was slightly lower (0.764 vs. 0.807), and centralization remained comparable (0.309 vs. 0.302). These metrics indicate that, under identical construction criteria, the Probio-M8 formula network contains more significant microbe-metabolite associations, exhibits tighter overall connectivity, and features more developed local cluster, while maintaining a relatively even distribution of connection strengths across nodes rather than being dominated by a few highly centralized hubs.

Discussion

The present work extends previously reported growth-related findings from the same preschool cohort[40] by leveraging the original trial infrastructure to integrate paired oral and gut microbiome profiling, gut resistome characterization, and fecal metabolomics. We treat growth and infection-related outcomes as key clinical readouts and use these multi-omics layers to contextualize how Probio-M8 formula intake influences microbiome organization, antimicrobial resistance potential, and host metabolic adaptation.

A central observation is that Probio-M8 formula intake was associated with greater gains in height and FFM over two months,[52-54] without a detectable upward shift in BMI at the group level.[55] This pattern aligns with a more favorable body composition trajectory than would be expected from energy supplementation alone, although the study design does not isolate which specific components of the formula contribute most strongly. Respiratory illness incidence did not differ between groups at individual time points, whereas antibiotic use was lower in the intervention group during early follow-up, with this difference attenuating by month 2. These endpoints are strongly shaped by exposure intensity, care-seeking behavior, and prescribing practices in kindergarten settings;[56-58] accordingly, we treat them as contextual readouts rather than direct measures of infectious biology. Within this constraint, the early divergence in antibiotic use is notable because

it provides a clinically proximate signal that can be evaluated alongside concurrent shifts in the gut ecosystem and resistome.[56,59]

The multi-omics data reveal that Probio-M8 formula intake was accompanied by site-specific remodeling of oral and gut communities, together with reduced coupling between these habitats.[60] Across the cohort, taxa detected in both saliva and stool represented only a small fraction of total microbial abundance at each site, and this shared fraction remained broadly stable over time. Against this background, the decline in oral-gut similarity and the weakening of cross-site concordance among shared taxa in the intervention group suggest a progressive reduction in coordinated fluctuations across body sites.[61,62] A parsimonious ecological interpretation is strengthened site differentiation, consistent with niche specialization and compartmentalization across mucosal habitats.[24] Importantly, this is a community-level inference and not a direct measurement of microbial migration. The observation nevertheless provides a quantitative handle on the oral-gut axis, which has been difficult to assess longitudinally in healthy preschool populations.

Diversity patterns further support divergent trajectories in saliva and stool. Oral alpha diversity decreased after Probio-M8 formula initiation, whereas gut alpha diversity showed a transient increase at week 2, returning toward control levels by month 2. Such site-specific responses are biologically plausible: oral communities are constrained by constant salivary flow, oxygen exposure, and host antimicrobial factors,[63] while the gut microbiome is shaped by substrate availability, anaerobiosis, bile acids, and community resistance.[64,65] In this framework, the early expansion in gut diversity may reflect short-term ecological accommodation to altered nutrient inputs, followed by consolidation as the ecosystem converges toward a new equilibrium.[66,67 61,68-70]

At the species level, Probio-M8 formula intake was associated with a focused set of changes in both saliva and stool. In saliva, several taxa, including *Mogibacterium diversum*, *Porphyromonas* sp003640335, and *Rothia mucilaginosa*, declined over follow-up. Several streptococcal taxa (*S. oralis*, *S. parasanguinis*, and *S. pseudopneumoniae*) also shifted in abundance. These changes are compositional and should not be interpreted as evidence that any single species directly determine respiratory outcomes. In stool, Probio-M8 formula intake was associated with enrichment of *B. animalis* and coordinated changes in other commensals, while taxa such as *Eisenbergiella tayi* and *Megasphaera micronuciformis* were reduced by month 2. Collectively, these patterns are consistent with a gut community that becomes more bifidobacteria-enriched during the intervention, alongside a decline in select taxa that are infrequently observed among core members of the healthy preschool gut microbiome. Whether these shifts reflect durable ecological replacement, altered metabolic niches, or indirect effects of reduced antibiotic exposure remains to be determined.[71-73]

A second mechanistic layer is the gut resistome. Using PathoFact annotation, we observed a consistent downshift of 29 ARGs in the intervention group, with prominent reductions among multidrug efflux component-encoding genes. There was also an overall reweighting of resistance mechanism categories. Two non-exclusive explanations merit consideration. First, lower antibiotic exposure during early follow-up may have lowered selective pressure, favoring contraction of resistance-linked features. Second, ecological and functional reprogramming of the gut community, driven by bifidobacteria enrichment and shifts in carbohydrate-active and metabolic modules, may have altered the abundance distribution of taxa that typically harbor specific resistance determinants. While the current data cannot establish directionality, the co-occurrence of early reductions in antibiotic use and a net contraction of resistance gene features supports a coherent, testable hypothesis: nutritional microbiome modulation may help steer preschool children toward a lower

antimicrobial resistance burden, without inducing detectable enrichment of high-risk resistance profiles.[58,74,75]

The fecal metabolome provides a time-resolved complement these community and resistome dynamics.[76] The intervention elicited a biphasic metabolic response: the greatest separation between groups occurred at week 2, followed by a more selective profile at month 2. Early signatures involved amino acid and central energy metabolism, alongside pathways annotated to mucosal immune processes. By month 2, the signal shifted toward lipid mediator remodeling and annotations related to neuroactive and immune functions, marked by increased levels of specialized pro-resolving mediators (e.g., resolvin D2) and multiple neuroactive compounds. These patterns are consistent with an early adaptation phase characterized by broad metabolic mobilization, followed by a later, signaling-oriented phase focused on homeostatic refinement. Given that untargeted metabolite annotations carry inherent uncertainty and that pathway databases are developed from diverse biological contexts, these results should be interpreted as mechanistic leads rather than definitive evidence of pathway activation. The time dependence itself is informative, suggesting that short-term responses may not predict the eventual equilibrium state.[77]

Integrative correlation networks provide an additional organizational framework. Metabolite phenotype associations segregated into two modules: one centered on growth (height and FFM) and another on medication and illness (antibiotic use and respiratory events). Species-metabolite associations revealed that taxa enriched during Probio-M8 formula intake, particularly *B. animalis*, were more frequently linked to metabolites correlated with growth and less frequently connected to those associated with antibiotic use. In the combined multi-omics co-occurrence network, the intervention group displayed higher edge counts, greater density and clustering, and shorter path lengths under identical construction thresholds. These topology differences indicate a tighter co-variation structure within the intervention group, although they do not imply causality. Their value lies in highlighting multi-layer features that consistently co-vary with clinical outcome, and therefore merit prioritization for future mechanistic validation.[78-80]

This study has several limitations. The trial used cluster allocation in a kindergarten setting and was open-label in the field, which may introduce potential behavioral or reporting biases in illness and medication outcomes. The two-month follow-up period limits conclusions about the durability of microbiome, resistome, and metabolome changes. Baseline differences in age and stool form were present, and residual confounding from unmeasured dietary, household, or care-seeking factors cannot be excluded. Microbiome analyses relied primarily on relative abundances. While 2bRAD-M enabled efficient species-level resolution in oral samples, it lacks the depth of shotgun metagenomics for strain-level tracking and functional inference. Finally, the study did not include direct measures of mucosal immunity or epithelial barrier function. Future work could address these gaps by extending follow-up duration, using more tightly matched control formulas, tracking Probio-M8 at the strain level, and integrating mucosal immune markers with targeted metabolite panels to test specific pathways suggested by the current data.

In summary, our findings position the preschool period as a developmental window that is both measurable and modifiable in real world settings. Intake of Probio-M8 formula was associated with improved growth-related outcomes, without an apparent increase in BMI, alongside reduced oral-gut microbial coupling, a net contraction of gut resistance gene features, and a time-structured metabolome response. These convergent signals support a model in which probiotic-enriched nutrition may shape microbiome organization and metabolic adaptation during a vulnerable yet

actionable phase of early childhood, with potential implications for growth quality and antimicrobial exposure trajectories.

Materials and methods

Study design, participants, and ethics statement

We conducted a cluster randomized controlled trial in March 2023 at a kindergarten in Huangmei County, Hubei Province, China. Randomization was implemented at the classroom level. Children were assessed at three prespecified time points: baseline, 2 weeks after intervention initiation, and 2 months after intervention initiation. The study protocol was approved by the Chinese Registered Clinical Trial Ethics Review Committee (ChiECRCT20220044) and conducted in accordance with the Declaration of Helsinki. Written informed consent was obtained from parents or legal guardians prior to enrollment. A subset of growth-related outcomes from this cohort has been published previously.[40] The current analysis extends this work by incorporating oral microbiome profiling, fecal metagenomics-based resistome characterization, and fecal metabolomics, along with integrative analyses linking these multi-omics layers to growth- and infection-related outcomes.

Inclusion and exclusion criteria

Eligible participants were healthy preschool children aged 5-6 years who met prespecified anthropometric screening criteria, defined as height-for-age and weight-for-age *Z*-scores below the sex- and age-specific reference median. Exclusion criteria included: acute or chronic diarrhea; major systemic diseases (e.g., tuberculosis, HIV infection, kidney disease, chronic hepatitis, or chronic obstructive pulmonary disease); use of antibiotics, probiotics, prebiotics, or products containing probiotics or prebiotics within 15 days prior to enrollment; allergy to dairy products or any ingredient in the study formulas; and anticipated poor adherence, defined as missing more than two daily servings within any single week.

CONSORT flow and analysis sets

Of 373 children assessed for eligibility, 53 were excluded, and 320 were allocated to clusters. At the end of follow-up, 317 children completed the trial and were included in the overall analysis set. Due to missing age or sex information or incomplete questionnaire or anthropometric records, 301 children were included in the primary clinical phenotype analyses, consistent with the prespecified analysis set used in the prior publication.[40]

For omics analyses: fecal shotgun metagenomics included 886 samples from 310 participants (baseline: $n = 293$; week 2: $n = 289$; month 2: $n = 304$); salivary 2bRAD-M profiling included 913 samples from 310 participants (baseline: $n = 302$; week 2: $n = 307$; month 2: $n = 304$); fecal metabolomics included 887 samples from 311 participants (baseline: $n = 298$; week 2: $n = 287$; month 2: $n = 302$).

Randomization and masking

Cluster allocation was performed using block randomization at the classroom level, based on a computer-generated random sequence created by an independent statistician who was not involved in recruitment, intervention delivery, or outcome assessment. Due to the classroom-level nature of the intervention, participants and on-site staff could not be masked to group assignment. However, all biological samples were de-identified and assigned anonymous codes prior to laboratory

processing. Laboratory personnel and bioinformatic analysts remained blinded to group allocation throughout primary data generation and analysis.

Intervention and follow-up

The intervention product was a pediatric formula supplemented with Probio-M8, containing a minimum of 2×10^8 CFU per gram of powder. Children in the intervention group consumed the Probio-M8-enriched formula twice daily during routine kindergarten schedules for two months. Each serving consisted of 25 g of powder reconstituted in 200 mL of warm water and was administered under staff supervision. Children in the control group continued their usual intake of standard school milk (125 mL per serving), provided twice daily in accordance with the standard protocol of the kindergarten. Both groups received their assigned products at approximately 10:00 and 15:00 each day. Participants were asked to maintain their habitual diet throughout the follow-up period. Health status, respiratory illness episodes, and medication use, including antibiotics, were recorded prospectively by trained staff throughout the study.

Clinical assessments and questionnaires

Body weight and body composition were assessed using an InBody 770 analyzer (Biospace, South Korea) based on bioelectrical impedance analysis, with measurements performed by trained staff following standardized operating procedures. Parents or legal guardians completed questionnaires on baseline characteristics, gastrointestinal symptoms, and respiratory illness after receiving standardized instructions. Primary clinical endpoints were changes from baseline to month 2 in height, weight, and FFM. Secondary endpoints included gastrointestinal symptom profiles, respiratory illness occurrence, and antibiotic use.

Sample collection, transport, and storage

Stool and saliva samples were collected at baseline, week 2, and month 2. Stool samples were divided into two aliquots: one was immediately mixed with a fecal DNA stabilizer (Longseemed, Guangzhou, China) for shotgun metagenomics; the other was placed in an additive-free tube for metabolomic analysis. Saliva was collected under staff supervision approximately one hour after breakfast; children rinsed their mouths with water before collection. All samples were placed on ice immediately after collection, transported on dry ice, and stored at -80°C until processing. Sample identifiers and collection timestamps were recorded according to standard operating procedures.

Shotgun metagenomic sequencing and metagenomic processing

Genomic DNA was extracted from 0.5 g stabilized stool using a commercial kit (Tiangen Biotech Co., Ltd., Beijing, China). DNA integrity was assessed by agarose gel electrophoresis, purity by NanoDrop spectrophotometry, and concentration by Qubit fluorimetry (Thermo Fisher Scientific, Waltham, MA, USA). Libraries were prepared from 1 μg DNA fragmented to ~350 bp using Covaris sonicator. Standard library preparation steps, including end repair, A-tailing, adapter ligation, purification, and PCR amplification, were performed. Libraries were quality-controlled by Qubit fluorimetry, Agilent 2100 Bioanalyzer, and quantitative PCR, then pooled and sequenced on the BGI MGISEQ-T7 platform (BGI Genomics, Shenzhen, China).

Raw reads were adapter-trimmed and filtered using fastp, with reads < 60 nt removed. Host-derived reads were discarded by mapping to the human reference genome (GRCh38) using

Bowtie2.[81] Taxonomic profiling was performed using MetaPhlAn4.[82] Functional profiling was performed using HUMAnN3[83] against the MetaCyc database to obtain gene family and pathway abundances and coverage estimates.

For genome-resolved analyses, metagenomic assemblies were generated using MEGAHIT[84] and contigs ≥ 2000 bp were retained. Binning was performed independently with MetaBAT2[85] and VAMB,[86] and results were consolidated using DAS Tool.[87] Bin quality was assessed using CheckM2;[88] only bins with ≥ 80% completeness and ≤ 5% contamination were retained. Redundancy bins were dereplicated using dRep89 at a 95% average nucleotide identity threshold.[89] Taxonomic assignment was performed using GTDB-Tk[90] with the GTDB release202 reference database. Metagenome-assembled genome abundances were estimated using CoverM[91] based on read mapping with a 95% identity threshold. Antibiotic resistance genes and associated resistance mechanism were annotated from fecal metagenomes using PathoFact,[92] generating both gene- and mechanism-level profiles.

Oral microbiome profiling by 2bRAD-M

Saliva DNA was profiled using 2bRAD-M.[93] Genomic DNA (1 pg-200 ng) was digested with BcgI (NEB, Ipswich, MA, USA) at 37°C for 3 h and verified by agarose gel electrophoresis. Digestion products were ligated to library-specific adapters (Ada1 and Ada2) in the presence of ATP and T4 DNA ligase at 4°C for 16 h, followed by heat inactivation. Libraries were amplified using Phusion High-Fidelity DNA Polymerase (NEB) for 16-28 cycles. Fragments of ~100 bp were size-selected via polyacrylamide gel electrophoresis and recovered. A 7-cycle barcode PCR was performed, products were purified using QIAquick spin columns (QIAGEN GmbH, Hilden, Germany), and libraries were sequenced on an Illumina NovaSeq 6000 platform (Illumina Inc., San Diego, CA, USA).

Demultiplexed reads were quality-filtered using fastp, removing reads with > 8% ambiguous bases or > 20% low-quality bases (Q ≤ 20). Taxonomic profiling was performed using MAP2B[94] with a built-in 2bRAD tag database covering bacteria, fungi, and archaea. Species-level abundances were estimated based on sequencing coverage of species-specific tags.

Fecal metabolomics and data processing

For fecal metabolomics, 200 mg of stool was extracted with 600 µL of methanol containing an internal standard (2-chloro-L-phenylalanine, 4 ppm). Samples were vortexed, bead-beaten, sonicated, and centrifuged; supernatants were filtered through a 0.22 µm membrane for LC-MS analysis.

Chromatographic separation was performed on a Thermo Vanquish UHPLC system (Thermo Fisher Scientific, Waltham, MA, USA) equipped with an ACQUITY UPLC HSS T3 column (2.1 × 100 mm, 1.8 µm; Waters, Milford, MA, USA). The flow rate was 0.3 mL/min, column temperature was 40°C, and injection volume was 2 µL. In positive ionization mode, mobile phases consisted of (A) 0.1% formic acid in water and (B) 0.1% formic acid in acetonitrile. In negative mode, mobile phases were (A) 5 mM ammonium formate in water and (B) acetonitrile. Mass spectrometry was performed on a Thermo Orbitrap Exploris 120 (Thermo Fisher Scientific) in both positive and negative ionization modes. Full scan MS data were acquired at 60,000 resolution over *m/z* 100-1,000. Data-dependent MS2 acquisition used higher-energy collisional dissociation at 30% collision energy, 15,000 resolution, top-4 precursor selection, and dynamic exclusion.

Raw data files were converted to mzML format using ProteoWizard. Peak detection, alignment, and retention time correction were performed using XCMS. Peak areas were normalized using a support vector regression-based batch correction method. Features with > 50% missing values were filtered out, and poorly reproducible features (e.g., low signal-to-noise or high coefficient of variation in quality controls) were removed. Metabolite annotation integrated an in-house spectral library, public databases (e.g., HMDB, METLIN), and metDNA.[95] Data were median normalized, log-transformed, and autoscaled prior to analysis. Differential metabolites were selected based on fold change and statistical significance. Pathway enrichment and visualization were performed using MetaboAnalyst 6.0.[96]

Quantification and statistical analysis

All statistical analyses were performed in R (v4.0.5). Selected nonparametric significance tests leveraged scripts from the Parallel Meta Suite. Categorical variables were compared using chi-square tests. Between group comparisons of continuous outcomes employed Wilcoxon rank sum tests, while within-group paired comparisons used Wilcoxon rank-sum tests. A two-sided $P < 0.05$ was considered statistically significant unless otherwise specified.

Microbiome alpha diversity was assessed using the Shannon and Simpson indices. Beta diversity was calculated using Bray-Curtis dissimilarity and visualized using principal coordinates analysis and uniform manifold approximation and projection. Group differences in community structure were assessed using PERMANOVA. To characterize oral-gut microbial coordination, taxa detected in both saliva and stool were defined as the shared set. For each participant, oral-to-gut similarity was quantified using L2 distance calculated on the shared set, and oral-to-gut concordance was measured using Spearman correlation, capturing coordinated abundance variation across the two sites. Associations among microbes, metabolites, and host phenotypes were evaluated using Spearman correlation. Multivariable associations and differential features were identified using MaAsLin2 where appropriate. Key R packages used for analysis and visualization included vegan, optparse, umap, ggplot2, ggpubr, and pheatmap.

Data availability

The metagenomic sequencing data generated in this study have been deposited in the Genome Sequence Archive at the National Genomics Data Center, China National Center for Bioinformation/Beijing Institute of Genomics, Chinese Academy of Sciences, under accession number PRJCA054170 (https://ngdc.cncb.ac.cn).

Acknowledgements

This work was supported by the National Natural Science Foundation of China (32394053, 32372304, and 32502149) and China Postdoctoral Science Foundation (2024M761523, and BX20250338).

Ethics statement

The study adhered to the principles outlined in the Declaration of Helsinki for research involving human subjects. The study protocol was approved by the Chinese Registered Clinical Trial Ethics Review Committee (ChiECRCT-20220044). Written informed consent was obtained from parents or legal guardians of all participating children prior to enrollment.

Author Contributions

H.Z., Z.Y., Z.L., and W.Z. conceived and designed the study and supervised the project. M.Z., Y.D., and K.L. carried out the experiments. M.Z., and X.H. performed data processing and statistical analyses. M.Z., and X.H. drafted the manuscript with input from W.Z, Y.D., Y.M., X.Z., and X.Y. M.Z., X.H., and L.K. revised and edited the manuscript. All authors read and approved the final version of the manuscript.

References

1. Nunez, H., Nieto, P.A., Mars, R.A., Ghavami, M., Sew Hoy, C., and Sukhum, K. (2025). Early life gut microbiome and its impact on childhood health and chronic conditions. Gut Microbes *17*, 2463567. https://doi.org/10.1080/19490976.2025.2463567.
2. Donald, K., and Finlay, B.B. (2023). Early-life interactions between the microbiota and immune system: Impact on immune system development and atopic disease. Nat. Rev. Immunol. *23*, 735-748. https://doi.org/10.1038/s41577-023-00874-w.
3. Almalki, S.N., Alhujaili, R.M., Althubyani, S.A., Alahmadi, W.T., Mustafa, S.A., Asiri, A.A., Alahmadi, R.O., Felemban, M.S., Alsogaihi, J.M., Alshehri, S.A., et al. (2024). Influence of early childhood education programmes on child development metrics: A systematic review and meta-analysis of randomised controlled trials. J. Adv. Trends Med. Res. *1*, 466-473. https://doi.org/10.4103/atmr.Atmr_180_24.
4. Draper, C.E., Yousafzai, A.K., McCoy, D.C., Cuartas, J., Obradović, J., Bhopal, S., Fisher, J., Jeong, J., Klingberg, S., Milner, K., et al. (2024). The next 1000 days: Building on early investments for the health and development of young children. Lancet *404*, 2094-2116. https://doi.org/10.1016/s0140-6736(24)01389-8.
5. Wilkie, E.D., Alao, J.O., Thonda, O.A., and Oluduro, A.O. (2024). Prevalence, distribution, and antibiotic resistance of bacterial isolates in daycare centers in Ile-Ife, Nigeria. Antimicrob. Steward. Healthc. Epidemiol. *4*, e220, e220. https://doi.org/10.1017/ash.2024.473.
6. Zhou, B., Niu, W., Liu, F., Yuan, Y., Wang, K., Zhang, J., Wang, Y., and Zhang, Z. (2021). Risk factors for recurrent respiratory tract infection in preschool-aged children. Pediatr. Res. *90*, 223-231. https://doi.org/10.1038/s41390-020-01233-4.
7. van Hecke, O., Fuller, A., Bankhead, C., Jenkins-Jones, S., Francis, N., Moore, M., Butler, C., and Wang, K. (2019). Antibiotic exposure and 'response failure' for subsequent respiratory tract infections: An observational cohort study of UK preschool children in primary care. Br. J. Gen. Pract. *69*, e638-e646. https://doi.org/10.3399/bjgp19X705089.
8. Brown, J.A., Bashir, H., and Zeng, M.Y. (2025). Lifelong partners: Gut microbiota-immune cell interactions from infancy to old age. Mucosal Immunol. *18*, 509-523. https://doi.org/10.1016/j.mucimm.2025.01.006.
9. Iliev, I.D., Blander, J.M., Collins, N., Guo, C.-J., Longman, R.S., Sonnenberg, G.F., Zeng, M.Y., and Artis, D. (2025). Microbiota-mediated mechanisms of mucosal immunity across the lifespan. Nat. Immunol. *26*, 1645-1659. https://doi.org/10.1038/s41590-025-02281-w.
10. Roberts, M., Tolar-Peterson, T., Reynolds, A., Wall, C., Reeder, N., and Rico Mendez, G. (2022). The effects of nutritional interventions on the cognitive development of preschool-age children: A systematic review. Nutrients *14*, 532. https://doi.org/10.3390/nu14030532.
11. Patrick, D.M., Sbihi, H., Dai, D.L.Y., Al Mamun, A., Rasali, D., Rose, C., Marra, F., Boutin, R.C.T., Petersen, C., Stiemsma, L.T., et al. (2020). Decreasing antibiotic use, the gut microbiota, and asthma incidence in children: Evidence from population-based and prospective cohort studies. Lancet Respir. Med. *8*, 1094-1105. https://doi.org/10.1016/S2213-2600(20)30052-7.
12. Zhu, M., Wang, Q., Yang, Y., Liu, X., Zhang, J., Li, G., Liu, W., Xiang, X., and Chen, J. (2025). Multiomics approach reveals the comprehensive interactions between nutrition and children's gut microbiota, and microbial and host metabolomes. Nutr. J. *24*, 50. https://doi.org/10.1186/s12937-025-01116-6.
13. Lv, H., Zhang, L., Han, Y., Wu, L., and Wang, B. (2022). The development of early life microbiota in human health and disease. Engineering *12*, 101-114. https://doi.org/https://doi.org/10.1016/j.eng.2020.12.014.
14. Ovaska, M., Tamminen, M., Lahdenperä, M., Vahtera, J., Rautava, S., Gonzales-Inca, C., Heiskanen, M.A., and Lagström, H. (2024). The role of early life factors and green living environment in the development of gut microbiota in infancy: Population-based cohort study. Environ. Int. *193*, 109093. https://doi.org/https://doi.org/10.1016/j.envint.2024.109093.
15. Wang, D., Pham, V.T., Steinert, R.E., Zhernakova, A., and Fu, J. (2022). Microbial vitamin production mediates dietary effects on diabetic risk. Gut Microbes *14*, 2154550. https://doi.org/10.1080/19490976.2022.2154550.
16. Shen, Y., Fan, N., Ma, S.-x., Cheng, X., Yang, X., and Wang, G. (2025). Gut microbiota dysbiosis: Pathogenesis, diseases, prevention, and therapy. Med. Comm. *6*, e70168. https://doi.org/https://doi.org/10.1002/mco2.70168.
17. Madhogaria, B., Bhowmik, P., and Kundu, A. (2022). Correlation between human gut microbiome and diseases. Infect. Med. (Beijing) *1*, 180-191. https://doi.org/https://doi.org/10.1016/j.imj.2022.08.004.
18. Jiang, Y., and Li, Y. (2025). The role of nutrition and gut microbiome in childhood brain

development and behavior. Front. Nutr. *12*, 1590172. https://doi.org/10.3389/fnut.2025.1590172.
19. Bankole, T., and Li, Y. (2025). The early-life gut microbiome in common pediatric diseases: Roles and therapeutic implications. Front. Nutr. *12*, 1597206. https://doi.org/10.3389/fnut.2025.1597206.
20. Verma, D., Garg, P.K., and Dubey, A.K. (2018). Insights into the human oral microbiome. Arch. Microbiol. *200*, 525-540. https://doi.org/10.1007/s00203-018-1505-3.
21. Kitamoto, S., Nagao-Kitamoto, H., Hein, R., Schmidt, T.M., and Kamada, N. (2020). The bacterial connection between the oral cavity and the gut diseases. J. Dent. Res. *99*, 1021-1029. https://doi.org/10.1177/0022034520924633.
22. Xu, Q., Wang, W., Li, Y., Cui, J., Zhu, M., Liu, Y., and Liu, Y. (2025). The oral-gut microbiota axis: A link in cardiometabolic diseases. NPJ Biofilms Microbiomes *11*, 11. https://doi.org/10.1038/s41522-025-00646-5.
23. Kunath, B.J., De Rudder, C., Laczny, C.C., Letellier, E., and Wilmes, P. (2024). The oral–gut microbiome axis in health and disease. Nat. Rev. Microbiol. *22*, 791-805. https://doi.org/10.1038/s41579-024-01075-5.
24. Azzolino, D., Carnevale-Schianca, M., Santacroce, L., Colella, M., Felicetti, A., Terranova, L., Castrejón-Pérez, R.C., Garcia-Godoy, F., Lucchi, T., and Passarelli, P.C. (2025). The oral–gut microbiota axis across the lifespan: New insights on a forgotten interaction. Nutrients *17*, 2538. https://doi.org/10.3390/nu17152538.
25. Lee, S., Arefaine, B., Begum, N., Stamouli, M., Witherden, E., Mohamad, M., Harzandi, A., Zamalloa, A., Cai, H., Williams, R., et al. (2025). Oral-gut microbiome interactions in advanced cirrhosis: Characterisation of pathogenic enterotypes and salivatypes, virulence factors and antimicrobial resistance. J. Hepatol. *82*, 622-633. https://doi.org/10.1016/j.jhep.2024.09.046.
26. Miyauchi, E., Taida, T., Uchiyama, K., Nakanishi, Y., Kato, T., Koido, S., Sasaki, N., Ohkusa, T., Sato, N., and Ohno, H. (2026). Smoking affects gut immune system of patients with inflammatory bowel diseases by modulating metabolomic profiles and mucosal microbiota. Gut *75*, 46-56. https://doi.org/10.1136/gutjnl-2025-334922.
27. Bao, J., Li, L., Zhang, Y., Wang, M., Chen, F., Ge, S., Chen, B., and Yan, F. (2022). Periodontitis may induce gut microbiota dysbiosis via salivary microbiota. Int. J. Oral Sci. *14*, 32. https://doi.org/10.1038/s41368-022-00183-3.
28. Liao, C., Rolling, T., Djukovic, A., Fei, T., Mishra, V., Liu, H., Lindberg, C., Dai, L., Zhai, B., Peled, J.U., et al. (2024). Oral bacteria relative abundance in faeces increases due to gut microbiota depletion and is linked with patient outcomes. Nat. Microbiol. *9*, 1555-1565. https://doi.org/10.1038/s41564-024-01680-3.
29. Jokela, R., Pärnänen, K.M.M., Ponsero, A.J., Lahti, L., Kolho, K.-L., de Vos, W.M., and Salonen, A. (2024). A cohort study in family triads: Impact of gut microbiota composition and early life exposures on intestinal resistome during the first two years of life. Gut Microbes *16*, 2383746. https://doi.org/10.1080/19490976.2024.2383746.
30. Zhang, J., Lei, H., Huang, J., Wong, J.W.C., and Li, B. (2025). Co-occurrence and co-expression of antibiotic, biocide, and metal resistance genes with mobile genetic elements in microbial communities subjected to long-term antibiotic pressure: Novel insights from metagenomics and metatranscriptomics. J. Hazard. Mater. *489*, 137559. https://doi.org/https://doi.org/10.1016/j.jhazmat.2025.137559.
31. Shi, H., Newton, D.P., Nguyen, T.H., Estrela, S., Sanchez, J., Tu, M., Ho, P.-Y., Zeng, Q., DeFelice, B.C., Sonnenburg, J.L., and Huang, K.C. (2025). Nutrient competition predicts gut microbiome restructuring under drug perturbations. Cell *188*, 6971-6986.e6914. https://doi.org/10.1016/j.cell.2025.10.038.
32. Shayista, H., Prasad, M.N.N., Raj, S.N., Prasad, A., Lakshmi, S., Ranjini, H.K., Manju, K., Ravikumara, Chouhan, R.S., Khohlova, O.Y., et al. (2025). Complexity of antibiotic resistance and its impact on gut microbiota dynamics. Eng. Microbiol. *5*, 100187. https://doi.org/https://doi.org/10.1016/j.engmic.2024.100187.
33. Hill, C., Guarner, F., Reid, G., Gibson, G.R., Merenstein, D.J., Pot, B., Morelli, L., Canani, R.B., Flint, H.J., Salminen, S., et al. (2014). The international scientific sssociation for probiotics and prebiotics consensus statement on the scope and appropriate use of the term probiotic. Nat. Rev. Gastroenterol. Hepatol. *11*, 506-514. https://doi.org/10.1038/nrgastro.2014.66.
34. Arzamasov, A.A., Rodionov, D.A., Hibberd, M.C., Guruge, J.L., Kent, J.E., Kazanov, M.D., Leyn, S.A., Elane, M.L., Sejane, K., Furst, A., et al. (2025). Integrative genomic reconstruction reveals heterogeneity in carbohydrate utilization across human gut bifidobacteria. Nat. Microbiol. *10*, 2031-2047. https://doi.org/10.1038/s41564-025-02056-x.

35. Liu, A., Ma, T., Xu, N., Jin, H., Zhao, F., Kwok, L.-Y., Zhang, H., Zhang, S., and Sun, Z. (2021). Adjunctive probiotics alleviates asthmatic symptoms via modulating the gut microbiome and serum metabolome. Microbiol. Spectr. *9*, e00859-00821. https://doi.org/10.1128/Spectrum.00859-21.
36. Zhao, F., Guo, Z., Kwok, L.-Y., Zhao, Z., Wang, K., Li, Y., Sun, Z., Zhao, J., and Zhang, H. (2023). *Bifidobacterium lactis* Probio-M8 improves bone metabolism in patients with postmenopausal osteoporosis, possibly by modulating the gut microbiota. Eur. J. Nutr. *62*, 965-976. https://doi.org/10.1007/s00394-022-03042-3.
37. Dinleyici, E.C., Indrio, F., Szajewska, H., Hojsak, I., Salvatore, S., Mihatsch, W.A., Canani, R.B., Campoy, C., Domellöf, M., Francavilla, R., et al. (2025). Recommendations on the health outcomes of infant formula supplemented with biotics by the European society for pediatric gastroenterology, hepatology, and nutrition special interest group on gut microbiota and modifications. J. Pediatr. Gastroenterol. Nutr. https://doi.org/10.1002/jpn3.70195.
38. Mitra, M., Petit-Jean, A., Agrawal, R., Vaidya, U., Ganguly, S., and Hays, N.P. (2025). Safety and tolerance of infant formulas containing probiotics: A multicenter, randomised, controlled trial in healthy term infants. Benef. Microbes., 1-15. https://doi.org/10.1163/18762891-bja00100.
39. Chew, C., Matsuyama, M., Davies, P.S.W., Hill, R.J., Morrison, M., Martin, R., Codoñer, F.M., Knol, J., and Roeselers, G. (2024). A young child formula supplemented with a synbiotic mixture of scGOS/lcFOS and *Bifidobacterium breve* M-16V improves the gut microbiota and iron status in healthy toddlers. Front. Pediatr. *12*, 1193027. https://doi.org/10.3389/fped.2024.1193027.
40. Ma, Y., Zhou, Y., Guo, L., Yang, B., Bai, C., Chen, Y., Dai, G., Zhou, C., Duan, Y., and Yang, Z. (2024). Effects of children milk powder intervention on growth and development of preschool children. Food and Nutrition in China *30*, 17-22. https://doi.org/10.3969/j.issn.1006-9577.2024.06.004.
41. Xiao, L., Feng, M., Chen, C., Xiao, Q., Cui, Y., and Zhang, Y. (2025). Microenvironment-regulating drug delivery nanoparticles for treating and preventing typical biofilm-induced oral diseases. Adv. Mater. *37*, e2304982. https://doi.org/10.1002/adma.202304982.
42. Gao, Z., Chen, X., Wang, C., Song, J., Xu, J., Liu, X., Qian, Y., and Suo, H. (2024). New strategies and mechanisms for targeting *Streptococcus mutans* biofilm formation to prevent dental caries: A review. Microbiol. Res. *278*, 127526. https://doi.org/https://doi.org/10.1016/j.micres.2023.127526.
43. Bloch, S., Hager-Mair, F.F., Andrukhov, O., and Schäffer, C. (2024). Oral streptococci: Modulators of health and disease. Front. Cell. Infect. Microbiol. *14*, 1357631. https://doi.org/10.3389/fcimb.2024.1357631.
44. Nomura, K., Ishikawa, D., Okahara, K., Ito, S., Haga, K., Takahashi, M., Arakawa, A., Shibuya, T., Osada, T., Kuwahara-Arai, K., et al. (2021). Bacteroidetes species are correlated with disease activity in ulcerative colitis. J. Clin. Med. *10*. https://doi.org/10.3390/jcm10081749.
45. Su, Q., Wong, O.W.H., Lu, W., Wan, Y., Zhang, L., Xu, W., Li, M.K.T., Liu, C., Cheung, C.P., Ching, J.Y.L., et al. (2024). Multikingdom and functional gut microbiota markers for autism spectrum disorder. Nat. Microbiol. *9*, 2344-2355. https://doi.org/10.1038/s41564-024-01739-1.
46. Ni, Y., Qian, L., Siliceo, S.L., Long, X., Nychas, E., Liu, Y., Ismaiah, M.J., Leung, H., Zhang, L., Gao, Q., et al. (2023). Resistant starch decreases intrahepatic triglycerides in patients with NAFLD via gut microbiome alterations. Cell Metab. *35*, 1530-1547.e1538. https://doi.org/10.1016/j.cmet.2023.08.002.
47. Ryu, S.W., Moon, J.C., Oh, B.S., Yu, S.Y., Bak, J.E., Heo, E.S., Jeong, J.H., and Lee, J.H. (2023). Anti-obesity activity of human gut microbiota *Bacteroides stercoris* KGMB02265. Arch. Microbiol. *206*, 19. https://doi.org/10.1007/s00203-023-03750-2.
48. Christensen, L., Sørensen, C.V., Wøhlk, F.U., Kjølbæk, L., Astrup, A., Sanz, Y., Hjorth, M.F., and Benítez-Páez, A. (2020). Microbial enterotypes beyond genus level: Bacteroides species as a predictive biomarker for weight change upon controlled intervention with arabinoxylan oligosaccharides in overweight subjects. Gut Microbes *12*, 1847627. https://doi.org/10.1080/19490976.2020.1847627.
49. Yoon, H., Gerdes, L.A., Beigel, F., Sun, Y., Kövilein, J., Wang, J., Kuhlmann, T., Flierl-Hecht, A., Haller, D., Hohlfeld, R., et al. (2025). Multiple sclerosis and gut microbiota: Lachnospiraceae from the ileum of MS twins trigger MS-like disease in germfree transgenic mice-An unbiased functional study. Proc. Natl. Acad. Sci. U. S. A. *122*, e2419689122. https://doi.org/10.1073/pnas.2419689122.
50. Akhi, R., Lavrinienko, A., Hakula, M., Tjäderhane, L., Hindström, R., Nissinen, A., Wang, C.,

Auvinen, J., Kullaa, A.M., Ylöstalo, P., et al. (2025). Oral microbiome diversity associates with carotid intima media thickness in middle-aged male subjects. Commun. Med. (Lond) *5*, 66. https://doi.org/10.1038/s43856-025-00773-2.

51. Zhang, Z., Zhang, Y., Wu, A., Xu, C., and Li, Z. (2025). Will gut, oral, and vaginal microbiota influence the outcome of FET or be influenced by FET? A pilot study. mBio *16*, e00509-00525. https://doi.org/doi:10.1128/mbio.00509-25.
52. Wang, Q., Yang, Y., Xiao, Y., Liu, Z., Li, M., Yu, Y., Wang, N., Li, J., Li, X., Xu, C., et al. (2025). *Bifidobacterium animalis* subsp. *lactis* BL-11 promotes height growth in 3- to 7-year-Old children with below-average height: A self-controlled clinical trial. Clin. Nutr. *50*, 57-65. https://doi.org/10.1016/j.clnu.2025.05.001.
53. Liu, C., Yang, Y.-n., Guo, S., Cao, Y., Wang, L.-n., and Wu, C. (2025). Gut microbiota-mediated regulation of skeletal development: A review of mechanistic analysis and interventional strategies. J. Adv. Res. https://doi.org/https://doi.org/10.1016/j.jare.2025.07.033.
54. Yang, Y., Yang, J., Zhang, W., Zhou, L., Zhu, C., Zhang, X., Mao, Y., and Zhang, M. Host–microbiota interaction drives 5-hydroxyindole-3-acetic acid production to promote linear growth in infant mice. iMetaOmics, e70062. https://doi.org/https://doi.org/10.1002/imo2.70062.
55. Zhang, M., Ding, L., Strodl, E., Yin, X., Wen, G., Sun, D., Xian, D., Zhao, Y., Zheng, Y., Liu, F., et al. (2025). Early supplement of probiotics reduces the risk of obesity among preschool children: A real-world observational study. Front. Nutr. *12*. https://doi.org/10.3389/fnut.2025.1597894.
56. Heston, S.M., Young, R.R., Jenkins, K., Martin, P.L., Stokhuyzen, A., Ward, D.V., Bhattarai, S.K., Bucci, V., Arshad, M., Chao, N.J., et al. (2024). The effects of antibiotic exposures on the gut resistome during hematopoietic cell transplantation in children. Gut Microbes *16*, 2333748. https://doi.org/10.1080/19490976.2024.2333748.
57. Sehgal, N., Pajuelo, M.J., Gilman, R.H., Pickering, A.J., Earl, A.M., Worby, C.J., and Nadimpalli, M.L. (2025). Effects of commonly used antibiotics on children's developing gut microbiomes and resistomes in peri-urban Lima, Peru. J. Antimicrob. Chemother. *80*, 3248-3256. https://doi.org/10.1093/jac/dkaf358.
58. Li, S., Liu, J., Zhang, X., Gu, Q., Wu, Y., Tao, X., Tian, T., Pan, G., and Chu, M. (2025). The potential impact of antibiotic exposure on the microbiome and human health. Microorganisms *13*, 602. https://doi.org/10.3390/microorganisms13030602.
59. Zhao, L., Yang, X., Liang, Y., Zhang, Z., Ding, Y., Wang, Y., Chen, B., Wu, J., Jin, C., Zhao, G., et al. (2024). Temporal development and potential interactions between the gut microbiome and resistome in early childhood. Microbiol. Spectr. *12*, e0317723. https://doi.org/10.1128/spectrum.03177-23.
60. Ma, Z., Zuo, T., Frey, N., and Rangrez, A.Y. (2024). A systematic framework for understanding the microbiome in human health and disease: From basic principles to clinical translation. Signal. Transduct. Target. Ther. *9*, 237. https://doi.org/10.1038/s41392-024-01946-6.
61. Costa, C., Correia-de-Sá, T., Araujo, R., Barbosa, F., Burnet, P.W.J., Ferreira-Gomes, J., and Sampaio-Maia, B. (2024). The oral-gut microbiota relationship in healthy humans: Identifying shared bacteria between environments and age groups. Front. Microbiol. *15*, 1475159. https://doi.org/10.3389/fmicb.2024.1475159.
62. Zhou, X., Shen, X., Johnson, J.S., Spakowicz, D.J., Agnello, M., Zhou, W., Avina, M., Honkala, A., Chleilat, F., Chen, S.J., et al. (2024). Longitudinal profiling of the microbiome at four body sites reveals core stability and individualized dynamics during health and disease. Cell Host Microbe *32*, 506-526.e509. https://doi.org/10.1016/j.chom.2024.02.012.
63. Rajasekaran, J.J., Krishnamurthy, H.K., Bosco, J., Jayaraman, V., Krishna, K., Wang, T., and Bei, K. (2024). Oral microbiome: A review of its impact on oral and systemic health. Microorganisms *12*, 1797. https://doi.org/10.3390/microorganisms12091797.
64. Meiners, F., Ortega-Matienzo, A., Fuellen, G., and Barrantes, I. (2025). Gut microbiome-mediated health effects of fiber and polyphenol-rich dietary interventions. Front. Nutr. *12*, 1647740. https://doi.org/10.3389/fnut.2025.1647740.
65. Bautista, J., Echeverría, C.E., Maldonado-Noboa, I., Ojeda-Mosquera, S., Hidalgo-Tinoco, C., and López-Cortés, A. (2025). The human microbiome in clinical translation: From bench to bedside. Front. Microbiol. *16*, 1632435. https://doi.org/10.3389/fmicb.2025.1632435.
66. Kang, J., Choi, Y., Keum, G.B., Doo, H., Kwak, J., Kim, H., Chae, Y., Lee, S., Yang, H., Kim, S., et al. (2025). Effect of diet and lifestyle changes on gut microbial diversity in healthy adolescents. J. Microbiol. Biotechnol. *35*, e2503018. https://doi.org/10.4014/jmb.2503.03018.
67. Fackelmann, G., Manghi, P., Carlino, N., Heidrich, V., Piccinno, G., Ricci, L., Piperni, E., Arrè, A., Bakker, E., Creedon, A.C., et al. (2025). Gut microbiome signatures of vegan, vegetarian

and omnivore diets and associated health outcomes across 21,561 individuals. Nat. Microbiol. *10*, 41-52. https://doi.org/10.1038/s41564-024-01870-z.

68. Rui, W., Zhong, S., Li, X., Tang, X., Wang, L., and Yang, J. (2025). Evaluating the role of postbiotics in the modulation of human oral microbiota: A randomized controlled clinical trial. Probiotics Antimicrob. Proteins *17*, 2942-2952. https://doi.org/10.1007/s12602-024-10238-y.
69. Baker, J.L., Mark Welch, J.L., Kauffman, K.M., McLean, J.S., and He, X. (2024). The oral microbiome: Diversity, biogeography and human health. Nat. Rev. Microbiol. *22*, 89-104. https://doi.org/10.1038/s41579-023-00963-6.
70. Hajishengallis, G., Lamont, R.J., and Koo, H. (2023). Oral polymicrobial communities: Assembly, function, and impact on diseases. Cell Host Microbe *31*, 528-538. https://doi.org/10.1016/j.chom.2023.02.009.
71. Yartey, S.N., Awere-Duodu, A., Asantewaa, A.A., and Donkor, E.S. (2025). Antibiotic impact on human microecology in low- and middle-income countries: A systematic age-stratified review of gut and respiratory microbiome and resistome. Ther. Adv. Infect. Dis. *12*, 20499361251389738. https://doi.org/10.1177/20499361251389738.
72. Lathakumari, R.H., Vajravelu, L.K., Satheesan, A., Ravi, S., and Thulukanam, J. (2024). Antibiotics and the gut microbiome: Understanding the impact on human health. Med. Microbiol. *20*, 100106. https://doi.org/https://doi.org/10.1016/j.medmic.2024.100106.
73. Zhang, Y., Xue, G., Wang, F., Zhang, J., Xu, L., and Yu, C. (2024). The impact of antibiotic exposure on antibiotic resistance gene dynamics in the gut microbiota of inflammatory bowel disease patients. Front. Microbiol. *15*, 1382332. https://doi.org/10.3389/fmicb.2024.1382332.
74. Kiu, R., Darby, E.M., Alcon-Giner, C., Acuna-Gonzalez, A., Camargo, A., Lamberte, L.E., Phillips, S., Sim, K., Shaw, A.G., Clarke, P., et al. (2025). Impact of early life antibiotic and probiotic treatment on gut microbiome and resistome of very-low-birth-weight preterm infants. Nat. Commun. *16*, 7569. https://doi.org/10.1038/s41467-025-62584-2.
75. Nogacka, A.M., Saturio, S., Alvarado-Jasso, G.M., Salazar, N., de los Reyes Gavilán, C.G., Martínez-Faedo, C., Suarez, A., Wang, R., Miyazawa, K., Harata, G., et al. (2024). Probiotic-induced modulation of microbiota composition and antibiotic resistance genes Load, an in vitro assessment. Int. J. Mol. Sci. *25*, 1003. https://doi.org/10.3390/ijms25021003.
76. Sangermani, M., Desiati, I., Jørgensen, S.M., Li, J.V., Andreassen, T., Bathen, T.F., and Giskeødegård, G.F. (2024). Stability in fecal metabolites amid a diverse gut microbiome composition: A one-month longitudinal study of variability in healthy individuals. Gut Microbes *16*, 2427878. https://doi.org/10.1080/19490976.2024.2427878.
77. Pan, R., Guo, M., Chen, Y., Lin, G., Tian, P., Wang, L., Zhao, J., Chen, W., and Wang, G. (2024). Dynamics of the gut microbiota and faecal and serum metabolomes during pregnancy—A longitudinal study. Nutrients *16*, 483. https://doi.org/10.3390/nu16040483.
78. Muller, E., Shiryan, I., and Borenstein, E. (2024). Multi-omic integration of microbiome data for identifying disease-associated modules. Nat. Commun. *15*, 2621. https://doi.org/10.1038/s41467-024-46888-3.
79. Tegegne, H.A., and Savidge, T.C. (2025). Gut microbiome metagenomics in clinical practice: Bridging the gap between research and precision medicine. Gut Microbes *17*, 2569739. https://doi.org/10.1080/19490976.2025.2569739.
80. Sherwani, M.K., Ruuskanen, M.O., Feldner-Busztin, D., Nisantzis Firbas, P., Boza, G., Móréh, Á., Borman, T., Putu Erawijantari, P., Scheuring, I., Gopalakrishnan, S., and Lahti, L. (2025). Multi-omics time-series analysis in microbiome research: A systematic review. Brief. Bioinform. *26*, bbaf502. https://doi.org/10.1093/bib/bbaf502.
81. Langmead, B., and Salzberg, S.L. (2012). Fast gapped-read alignment with Bowtie 2. Nat. Methods *9*, 357-359. https://doi.org/10.1038/nmeth.1923.
82. Blanco-Míguez, A., Beghini, F., Cumbo, F., McIver, L.J., Thompson, K.N., Zolfo, M., Manghi, P., Dubois, L., Huang, K.D., Thomas, A.M., et al. (2023). Extending and improving metagenomic taxonomic profiling with uncharacterized species using MetaPhlAn 4. Nat. Biotechnol. *41*, 1633-1644. https://doi.org/10.1038/s41587-023-01688-w.
83. Franzosa, E.A., McIver, L.J., Rahnavard, G., Thompson, L.R., Schirmer, M., Weingart, G., Lipson, K.S., Knight, R., Caporaso, J.G., Segata, N., and Huttenhower, C. (2018). Species-level functional profiling of metagenomes and metatranscriptomes. Nat. Methods *15*, 962-968. https://doi.org/10.1038/s41592-018-0176-y.
84. Li, D., Liu, C.-M., Luo, R., Sadakane, K., and Lam, T.-W. (2015). MEGAHIT: An ultra-fast single-node solution for large and complex metagenomics assembly via succinct *de Bruijn* graph. Bioinformatics *31*, 1674-1676. https://doi.org/10.1093/bioinformatics/btv033.
85. Kang, D.D., Li, F., Kirton, E., Thomas, A., Egan, R., An, H., and Wang, Z. (2019). MetaBAT 2:

An adaptive binning algorithm for robust and efficient genome reconstruction from metagenome assemblies. PeerJ *7*, e7359. https://doi.org/10.7717/peerj.7359.

86. Nissen, J.N., Johansen, J., Allesøe, R.L., Sønderby, C.K., Armenteros, J.J.A., Grønbech, C.H., Jensen, L.J., Nielsen, H.B., Petersen, T.N., Winther, O., and Rasmussen, S. (2021). Improved metagenome binning and assembly using deep variational autoencoders. Nat. Biotechnol. *39*, 555-560. https://doi.org/10.1038/s41587-020-00777-4.
87. Sieber, C.M.K., Probst, A.J., Sharrar, A., Thomas, B.C., Hess, M., Tringe, S.G., and Banfield, J.F. (2018). Recovery of genomes from metagenomes via a dereplication, aggregation and scoring strategy. Nat. Microbiol. *3*, 836-843. https://doi.org/10.1038/s41564-018-0171-1.
88. Parks, D.H., Imelfort, M., Skennerton, C.T., Hugenholtz, P., and Tyson, G.W. (2015). CheckM: Assessing the quality of microbial genomes recovered from isolates, single cells, and metagenomes. Genome Res. *25*, 1043-1055. https://doi.org/10.1101/gr.186072.114.
89. Olm, M.R., Brown, C.T., Brooks, B., and Banfield, J.F. (2017). dRep: A tool for fast and accurate genomic comparisons that enables improved genome recovery from metagenomes through de-replication. ISME J. *11*, 2864-2868. https://doi.org/10.1038/ismej.2017.126.
90. Chaumeil, P.-A., Mussig, A.J., Hugenholtz, P., and Parks, D.H. (2019). GTDB-Tk: A toolkit to classify genomes with the Genome Taxonomy Database. Bioinformatics *36*, 1925-1927. https://doi.org/10.1093/bioinformatics/btz848.
91. Aroney, S.T.N., Newell, R.J.P., Nissen, J.N., Camargo, A.P., Tyson, G.W., and Woodcroft, B.J. (2025). CoverM: Read alignment statistics for metagenomics. Bioinformatics *41*. https://doi.org/10.1093/bioinformatics/btaf147.
92. de Nies, L., Lopes, S., Busi, S.B., Galata, V., Heintz-Buschart, A., Laczny, C.C., May, P., and Wilmes, P. (2021). PathoFact: A pipeline for the prediction of virulence factors and antimicrobial resistance genes in metagenomic data. Microbiome *9*, 49. https://doi.org/10.1186/s40168-020-00993-9.
93. Sun, Z., Huang, S., Zhu, P., Tzehau, L., Zhao, H., Lv, J., Zhang, R., Zhou, L., Niu, Q., Wang, X., et al. (2022). Species-resolved sequencing of low-biomass or degraded microbiomes using 2bRAD-M. Genome Biol. *23*, 36. https://doi.org/10.1186/s13059-021-02576-9.
94. Sun, Z., Liu, J., Zhang, M., Wang, T., Huang, S., Weiss, S.T., and Liu, Y.Y. (2023). Removal of false positives in metagenomics-based taxonomy profiling via targeting Type IIB restriction sites. Nat. Commun. *14*, 5321. https://doi.org/10.1038/s41467-023-41099-8.
95. Zhang, H., Zeng, X., Yin, Y., and Zhu, Z.-J. (2025). Knowledge and data-driven two-layer networking for accurate metabolite annotation in untargeted metabolomics. Nat. Commun. *16*, 8118. https://doi.org/10.1038/s41467-025-63536-6.
96. Xia, J., and Wishart, D.S. (2011). Web-based inference of biological patterns, functions and pathways from metabolomic data using MetaboAnalyst. Nat. Protoc. *6*, 743-760. https://doi.org/10.1038/nprot.2011.319.

Table Legends

Table 1. Baseline characteristics and longitudinal clinical outcomes of preschool children in the intervention and control groups

Index		Intervention (*n* = 167)			Control (*n* = 134)			*P*-value		
Time points		Baseline	2 wks	2 mos	0 week	2 wks	2 mos	Baseline	2 wks	2 mos
Age (mean ± SD)		5.77 ± 0.45			5.66 ± 0.52			< 0.01		
Sex *n* (%)	Male	95 (57)			68 (51)			0.310		
	Female	72 (43)			66 (49)					
Premature infant *n* (%)	N	156 (93)			119 (89)			0.157		
	Y	11 (7)			15 (11)					
Delivery mode *n* (%)	C-section	82 (49)			72 (54)			0.425		
	Eutocia	85 (51)			62 (46)					
Mode of feeding	Breastfeeding	150 (90)			122 (92)			0.572		
	Non-breastfeeding	17 (10)			11 (8)					
Height (mean ± SD)		114.70 ± 5.50	/	116.43 ± 5.49	113.81 ± 6.03	/	115.14 ± 5.99	0.100	/	0.029
Weight (mean ± SD)		21.19 ± 3.11	/	21.62 ± 3.31	20.95 ± 4.09	/	21.27 ± 4.32	0.062	/	0.036
BMI (mean ± SD)		16.02 ± 1.59	/	15.87 ± 1.67	16.1 ± 1.95	/	15.96 ± 2.05	0.600	/	0.580
FFM (mean ± SD)		17.23 ± 2.06	/	17.76 ± 2.13	16.89 ± 2.36	/	17.32 ± 2.39	0.053	/	0.021
Food allergy *n* (%)	N	143 (86)	130 (87)	140 (89)	112 (84)	102 (84)	102 (82)	0.624	0.396	0.129
	Y	24 (14)	19 (13)	18 (11)	22 (16)	20 (16)	22 (18)			
Allergic diseases *n* (%)	N	127 (76)	123 (74)	124 (74)	93 (69)	90 (67)	90 (67)	0.196	0.219	0.178
	Y	40 (24)	44 (26)	43 (26)	41 (31)	44 (33)	44 (33)			
Eczema *n* (%)	N	138 (83)	142 (85)	141 (84)	109 (81)	104 (78)	105 (78)	0.772	0.098	0.175
	Y	29 (17)	25 (15)	26 (16)	25 (19)	30 (22)	29 (22)			
Asthma *n* (%)	N	164 (98)	164 (98)	163 (98)	132 (99)	132 (98)	133 (99)	0.838	0.792	0.266
	Y	3 (2)	3 (2)	4 (2)	2 (1)	3 (2)	1 (1)			
Atopic dermatitis *n* (%)	N	163 (98)	160 (96)	163 (98)	129 (96)	129 (96)	129 (96)	0.499	0.839	0.499
	Y	4 (2)	7 (4)	4 (2)	5 (4)	5 (4)	5 (4)			
Rhinitis *n* (%)	N	151 (90)	153 (92)	153 (92)	116 (87)	113 (84)	114 (85)	0.294	0.049	0.075
	Y	16 (10)	14 (8)	14 (8)	18 (13)	21 (16)	20 (15)			
Defecation *n* (%)	1 time	160 (96)	166 (99)	160 (96)	128 (96)	130 (97)	127 (95)	0.976	0.107	0.530
	2 times	5 (3)	1 (1)	6 (4)	4 (3)	4 (3)	7 (5)			
	⩾ 3 times	2 (1)	0	1 (0.6)	2 (1)	0	0			

Stool characteristics *n* (%)	Health	154 (92)	153 (92)	153 (92)	111 (83)	117 (87)	121 (90)	0.013	0.222	0.691
	Unhealth	13 (8)	14 (8)	14 (8)	23 (17)	17 (13)	13 (10)			
Respiratory illness *n* (%)	N	157 (94)	153 (92)	150 (90)	118 (88)	114 (86)	114 (86)	0.068	0.105	0.277
	Y	10 (6)	14 (8)	17 (10)	16 (12)	19 (14)	19 (14)			
Antibiotic use *n* (%)	N	162 (97)	157 (94)	145 (87)	120 (90)	110 (82)	109 (81)	0.008	0.001	0.193
	Y	5 (3)	10 (6)	22 (13)	14 (10)	24 (18)	25 (19)			

[a]Data are presented as mean ± SD or n (%). *P*-values compare the intervention and control groups at the same time point. For continuous variables (age, height, weight, body mass index [BMI], free-fat mass [FFM]), *P*-values were calculated using the Wilcoxon rank-sum test. For categorical variables, *P*-values were calculated using the χ^2 test. N = no; Y = yes.

Figures Legends

Figure 1. Study design and effects of Probio-M8 formula on growth in preschool children. (a) Schematic overview of the cluster randomized controlled trial and multi-omics workflow. Healthy preschool children were randomized by classroom to receive either Probio-M8-enriched formula (intervention group) or standard school milk (control group). Anthropometric measurements, body composition assessments, and questionnaire-based health data were collected baseline, 2 weeks (2 wks), and 2 months (2 mos). Concurrently, stool and saliva samples were collected at each time point. Saliva was profiled using 2bRAD-M; fecal microbial communities were characterized by shotgun metagenomics; and fecal metabolites were quantified by LC-MS. Multi-omics integration was used to link microbial and metabolite features to growth and infection-related clinical outcomes. **(b, c)** Longitudinal and net changes in height, weight, body mass index (BMI), and fat free mass (FFM) in the intervention and control groups from baseline to 2 months. Boxes indicate the interquartile range, with the horizontal line denoting the median. Whiskers extend to the most extreme data points within 1.5 × interquartile range of the lower and upper quartiles. Dots beyond the whiskers represent outliers. Overlaid lines indicate individual trajectories. Between-group differences were assessed using the Wilcoxon rank-sum test; * $P < 0.05$, ** $P < 0.01$, *** $P < 0.001$. In panel c, Δ represents the within-child change from baseline to 2 months (2 mos - baseline).

Figure 2. Effects of Probio-M8 formula on oral and gut microbiome structure, cross-site coupling, and functional profiles in preschool children. (a) Relative abundance of microbial taxa shared between saliva and stool in the intervention and control groups at baseline, 2 weeks (2 wks), and 2 months (2 mos). Error bars represent SEM. **(b)** Within-child oral-gut coupling for shared taxa.. Left, paired microbial similarity between saliva and stool profiles of shared species, quantified using L2 similarity. Right, within-child Spearman correlation of shared species abundances between oral and gut communities. Boxplots show the distribution at each time point by groups; asterisks denote significant between-group differences (*$P < 0.05$, **$P < 0.01$, Wilcoxon rank-sum test). **(c)** Alpha diversity of oral and gut microbiomes at each time point, measured by Shannon and Simpson indices. Boxes indicate the interquartile range, with the horizontal line denoting the median. Whiskers extend to the most extreme data points within 1.5 × interquartile range of the lower and upper quartiles. Dots beyond the whiskers represent outliers. Between-group differences were assessed using the Wilcoxon rank sum test; *$P < 0.05$, **$P < 0.01$, ***$P < 0.001$, and ****$P < 0.0001$. **(d)** Contribution of host and environmental factors to variation in microbial and functional profiles. PERMANOVA (Bray-Curtis dissimilarity) was applied separately to oral microbiome, gut microbiome, antibiotic resistance genes (ARG), carbohydrate-active enzyme (CAZy) family, Kyoto Encyclopedia of Genes and Genomes (KEGG) modules and pathways. The heatmap (left) highlights factors with significant effects ($P < 0.05$, red squares). The horizontal bar plot (right) shows PERMANOVA covariate effect (F statistics) for each factor. **(e)** Beta diversity of microbial and functional features in response to Probio-M8 formula administration. Principal coordinate analysis (PCoA; Bray-Curtis dissimilarity) are shown for oral microbiome, gut microbiome, ARG, CAZy, KEGG modules and pathways at the three time points. Ellipses indicate group-wise dispersion at each time point. The matrix (bottom right) summarizes PERMANOVA results comparing intervention and control groups at each time point.

Figure 3. Probio-M8 formula is associated with species-level remodeling of oral and gut microbiota and shifts in the gut resistome. (a) Circular heatmaps showing relative abundances of intervention-associated species in oral (top) and gut (bottom) microbiomes. Rings correspond to: intervention baseline, intervention week 2 (2 wks), intervention month 2 (2 mos), control baseline, control 2 wks, and control 2 mos. Color intensity reflects $\log_{10}$(relative abundance × 10^6). **(b)** Temporal dynamics of representative differentially abundant taxa in saliva and stool. Boxplots display $\log_{10}$-transformed relative abundances of selected oral and gut species. Boxes indicate the interquartile range, with the horizontal line denoting the median. Whiskers extend to the most extreme data points within 1.5 × interquartile range of the lower and upper quartiles. Dots beyond the whiskers represent outliers. Between-group differences at each time point were assessed using two-tailed Wilcoxon rank-sum test (*P < 0.05, **P < 0.01, ***P < 0.001). **(c)** Volcano plots of differentially abundant antibiotic resistance genes (ARGs) between intervention and control groups at the three time points. Green dots (Down): ARGs significantly lower in the intervention group; red dots (Up): ARGs significantly higher; grey dots (NS): non-significant differences. **(d)** Resistance mechanism-level summary of ARG abundance changes in the intervention group at week 2 and month 2 relative to baseline. Adjacent numbers denote the count of individual ARGs within each mechanism category that increased (red bars) or decreased (green bars) in abundance.

Figure 4. Probio-M8 formula is associated with time-dependent remodeling of the fecal metabolome in preschool children. (a) Volcano plots of differentially abundant fecal metabolites between the intervention and control groups at baseline, 2 weeks (2 wks), and 2 months (2 mos). Metabolites significantly increased in the intervention group are colored red (Up); those significantly decreased are colored green (Down). Significance was defined by P < 0.05 and a variable importance in projection score (VIP) > 1; dot size reflects VIP magnitude. Grey dots (ns) denote non-significant metabolites. **(b)** Venn diagram showing the number and overlap of discriminatory metabolites between intervention and control groups at the three time points. **(c)** Circular heatmap of 76 metabolites that showed consistent, intervention-associated changes across the trial. Rows correspond to individual metabolites; concentric segments represent intervention and time points. Color intensity reflects $\log_{10}$(relative abundance). **(d)** Pathway-level interpretation of metabolomic remodeling at 2 weeks and 2 months. Left: bubble plots of significantly enriched metabolic pathways; bubble size represents the number of matched metabolites (hits) and color encodes pathway significance. Right: corresponding metabolite-pathway networks highlighting key metabolites that connect multiple enriched pathways. Node color reflects the direction and magnitude of $\log_2$fold change, and node size represents the number of pathway hits.

Figure 5. Multi-omics association patterns and co-occurrence networks linking microbes, metabolites, and clinical readouts in preschool children receiving Probio-M8 formula. (a) Heatmap of Spearman rank correlations between host phenotypes and differentially abundant fecal metabolites. Columns represent clinical variables, growth and body composition measures (height, weight, fat-free mass), gastrointestinal and respiratory outcomes, and antibiotic use; rows correspond to metabolites significantly differing between intervention and control groups. **(b)** Heatmap of Spearman rank correlations between intervention-associated gut microbial species and differentially abundant fecal metabolites. Rows correspond to microbial species; columns refer to metabolites. In the heatmaps, color denotes the correlation coefficient (red, positive; blue,

negative; *P < 0.05, **P < 0.01). **(c)** Integrated multi-omics co-occurrence networks for the intervention and control groups, constructed from significant Spearman correlations among differential gut species, metabolites, and functional features including antibiotic resistance gene (ARG), carbohydrate-active enzyme (CAZy) family, Kyoto Encyclopedia of Genes and Genomes (KEGG) module and pathway, metabolite, and microbial species. Nodes represent biological entities, colored by data type and shaped by category. Edges reflect significant correlations meeting thresholds for effect size and P value (r > 0.4, P < 0.01), with line thickness proportional to the absolute correlation coefficient. Summary network metrics are reported beneath each network.

Figures

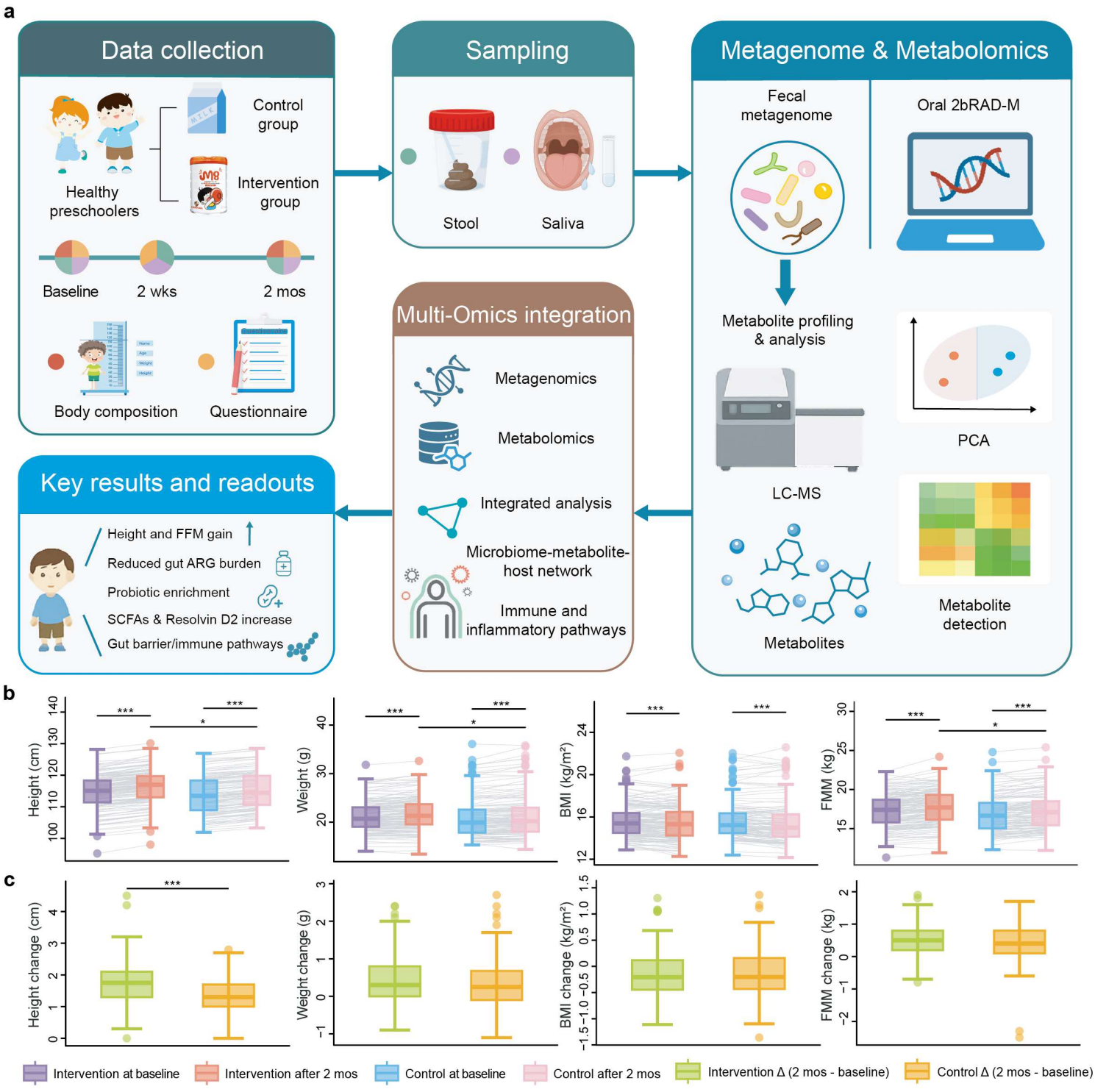


Figure 1

Study design and effects of Probio-M8 formula on growth in preschool children. (a) Schematic overview of the cluster randomized controlled trial and multi-omics workflow. Healthy preschool children were randomized by classroom to receive either Probio-M8-enriched formula (intervention group) or standard school milk (control group). Anthropometric measurements, body composition assessments,

and questionnaire-based health data were collected baseline, 2 weeks (2 wks), and 2 months (2 mos). Concurrently, stool and saliva samples were collected at each time point. Saliva was profiled using 2bRAD-M; fecal microbial communities were characterized by shotgun metagenomics; and fecal metabolites were quantified by LC-MS. Multi-omics integration was used to link microbial and metabolite features to growth and infection-related clinical outcomes. **(b, c)**Longitudinal and net changes in height, weight, body mass index (BMI), and fat free mass (FFM) in the intervention and control groups from baseline to 2 months. Boxes indicate the interquartile range, with the horizontal line denoting the median. Whiskers extend to the most extreme data points within 1.5 × interquartile range of the lower and upper quartiles. Dots beyond the whiskers represent outliers. Overlaid lines indicate individual trajectories. Between-group differences were assessed using the Wilcoxon rank-sum test; * $P < 0.05$, ** $P < 0.01$, *** $P < 0.001$. In panel c, Δ represents the within-child change from baseline to 2 months (2 mos - baseline).

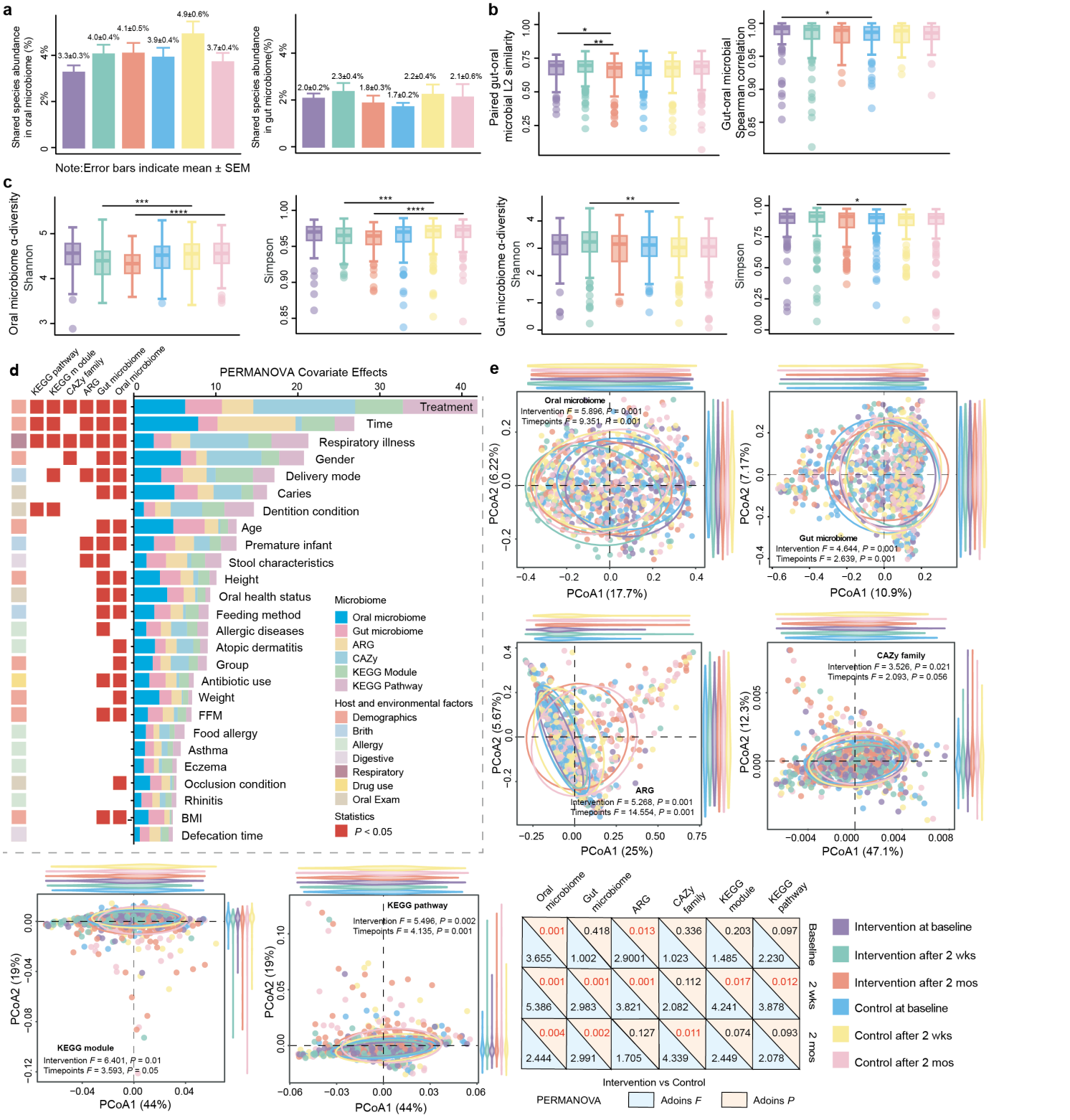


Figure 2

Effects of Probio-M8 formula on oral and gut microbiome structure, cross-site coupling, and functional profiles in preschool children. (a) Relative abundance of microbial taxa shared between saliva and stool in the intervention and control groups at baseline, 2 weeks (2 wks), and 2 months (2 mos). Error bars represent SEM. **(b)** Within-child oral-gut coupling for shared taxa.. Left, paired microbial similarity between saliva and stool profiles of shared species, quantified using L2 similarity. Right, within-child

Spearman correlation of shared species abundances between oral and gut communities. Boxplots show the distribution at each time point by groups; asterisks denote significant between-group differences (*P < 0.05, **P< 0.01, Wilcoxon rank-sum test). **(c)** Alpha diversity of oral and gut microbiomes at each time point, measured by Shannon and Simpson indices. Boxes indicate the interquartile range, with the horizontal line denoting the median. Whiskers extend to the most extreme data points within 1.5 × interquartile range of the lower and upper quartiles. Dots beyond the whiskers represent outliers. Between-group differences were assessed using the Wilcoxon rank sum test; *P < 0.05, **P < 0.01, ***P < 0.001, and ****P < 0.0001. **(d)** Contribution of host and environmental factors to variation in microbial and functional profiles. PERMANOVA (Bray-Curtis dissimilarity) was applied separately to oral microbiome, gut microbiome, antibiotic resistance genes (ARG), carbohydrate-active enzyme (CAZy) family, Kyoto Encyclopedia of Genes and Genomes (KEGG) modules and pathways. The heatmap (left) highlights factors with significant effects (P < 0.05, red squares). The horizontal bar plot (right) shows PERMANOVA covariate effect (Fstatistics) for each factor. **(e)** Beta diversity of microbial and functional features in response to Probio-M8 formula administration. Principal coordinate analysis (PCoA; Bray-Curtis dissimilarity) are shown for oral microbiome, gut microbiome, ARG, CAZy, KEGG modules and pathways at the three time points. Ellipses indicate group-wise dispersion at each time point. The matrix (bottom right) summarizes PERMANOVA results comparing intervention and control groups at each time point.

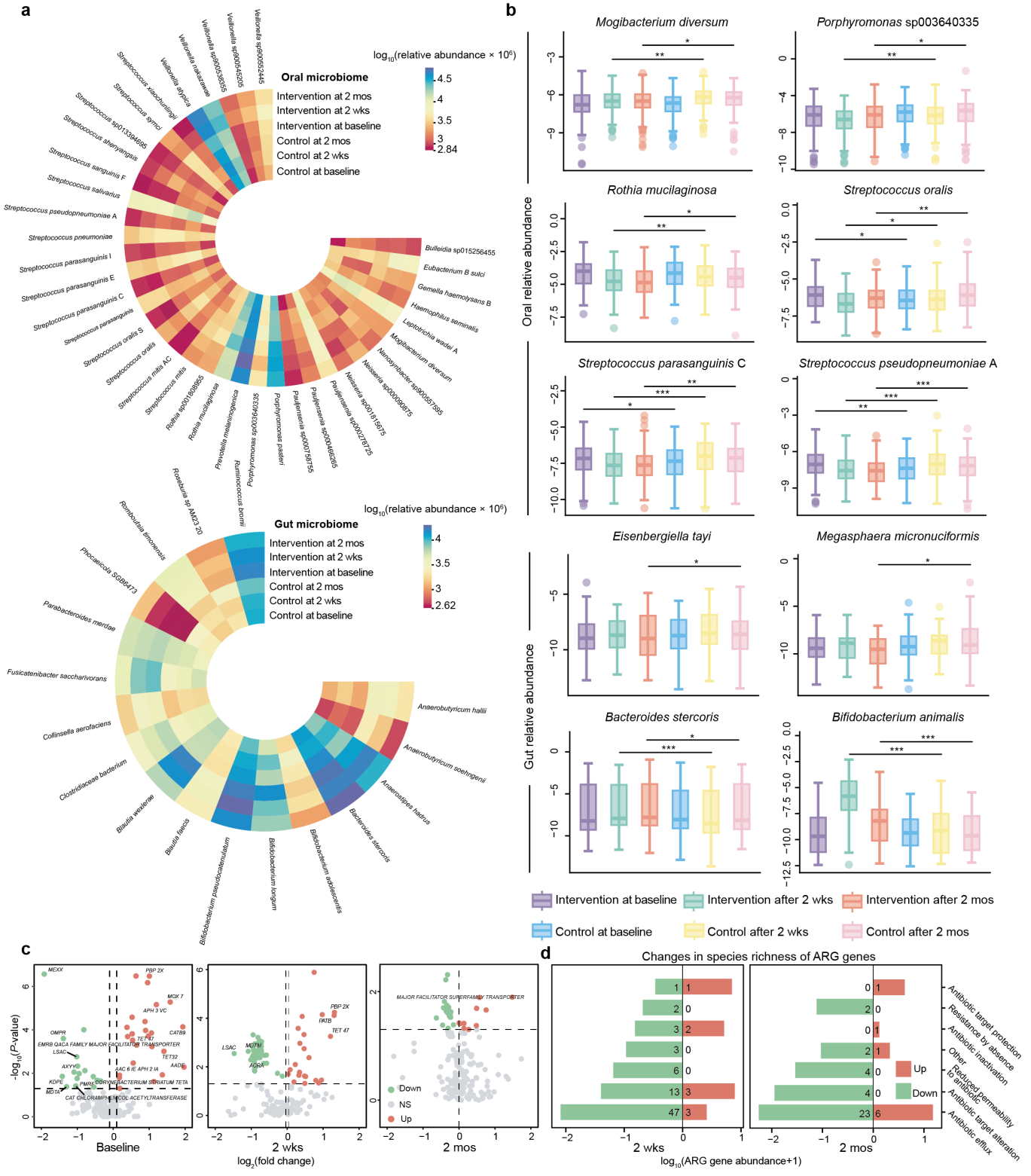


Figure 3

Probio-M8 formula is associated with species-level remodeling of oral and gut microbiota and shifts in the gut resistome. (a) Circular heatmaps showing relative abundances of intervention-associated species in oral (top) and gut (bottom) microbiomes. Rings correspond to: intervention baseline, intervention week 2 (2 wks), intervention month 2 (2 mos), control baseline, control 2 wks, and control 2 mos. Color intensity reflects $\log_{10}$(relative abundance × 10^6). **(b)** Temporal dynamics of representative

differentially abundant taxa in saliva and stool. Boxplots display $\log_{10}$-transformed relative abundances of selected oral and gut species. Boxes indicate the interquartile range, with the horizontal line denoting the median. Whiskers extend to the most extreme data points within 1.5 × interquartile range of the lower and upper quartiles. Dots beyond the whiskers represent outliers. Between-group differences at each time point were assessed using two-tailed Wilcoxon rank-sum test (*P < 0.05, **P < 0.01, ***P < 0.001). **(c)** Volcano plots of differentially abundant antibiotic resistance genes (ARGs) between intervention and control groups at the three time points. Green dots (Down): ARGs significantly lower in the intervention group; red dots (Up): ARGs significantly higher; grey dots (NS): non-significant differences. **(d)** Resistance mechanism-level summary of ARG abundance changes in the intervention group at week 2 and month 2 relative to baseline. Adjacent numbers denote the count of individual ARGs within each mechanism category that increased (red bars) or decreased (green bars) in abundance.

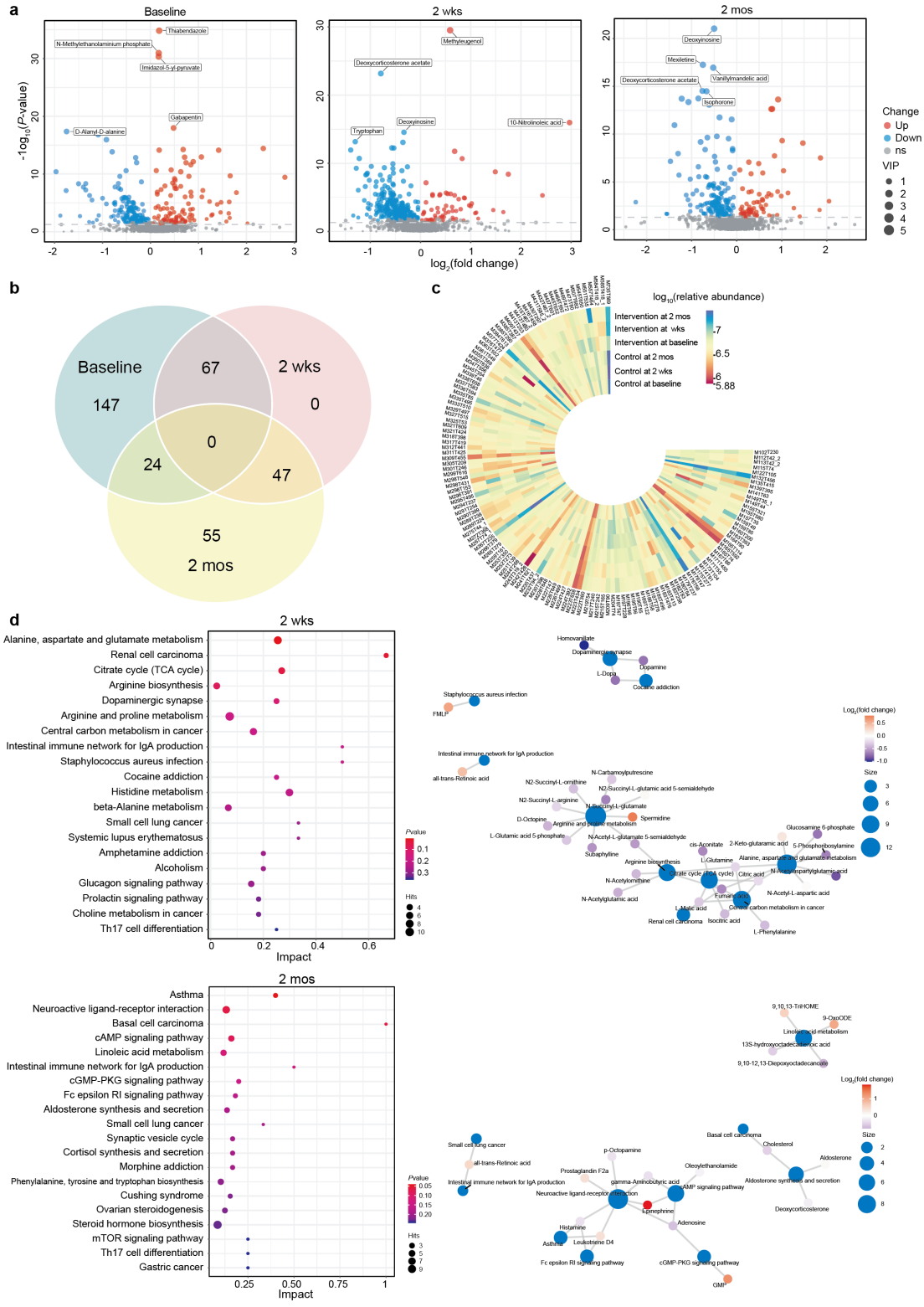


Figure 4

Probio-M8 formula is associated with time-dependent remodeling of the fecal metabolome in preschool children. (a) Volcano plots of differentially abundant fecal metabolites between the intervention and control groups at baseline, 2 weeks (2 wks), and 2 months (2 mos). Metabolites significantly increased in the intervention group are colored red (Up); those significantly decreased are colored green (Down). Significance was defined by $P < 0.05$ and a variable importance in projection

score (VIP) > 1; dot size reflects VIP magnitude. Grey dots (ns) denote non-significant metabolites. **(b)** Venn diagram showing the number and overlap of discriminatory metabolites between intervention and control groups at the three time points. **(c)** Circular heatmap of 76 metabolites that showed consistent, intervention-associated changes across the trial. Rows correspond to individual metabolites; concentric segments represent intervention and time points. Color intensity reflects $\log_{10}$(relative abundance). **(d)** Pathway-level interpretation of metabolomic remodeling at 2 weeks and 2 months. Left: bubble plots of significantly enriched metabolic pathways; bubble size represents the number of matched metabolites (hits) and color encodes pathway significance. Right: corresponding metabolite-pathway networks highlighting key metabolites that connect multiple enriched pathways. Node color reflects the direction and magnitude of $\log_2$fold change, and node size represents the number of pathway hits.

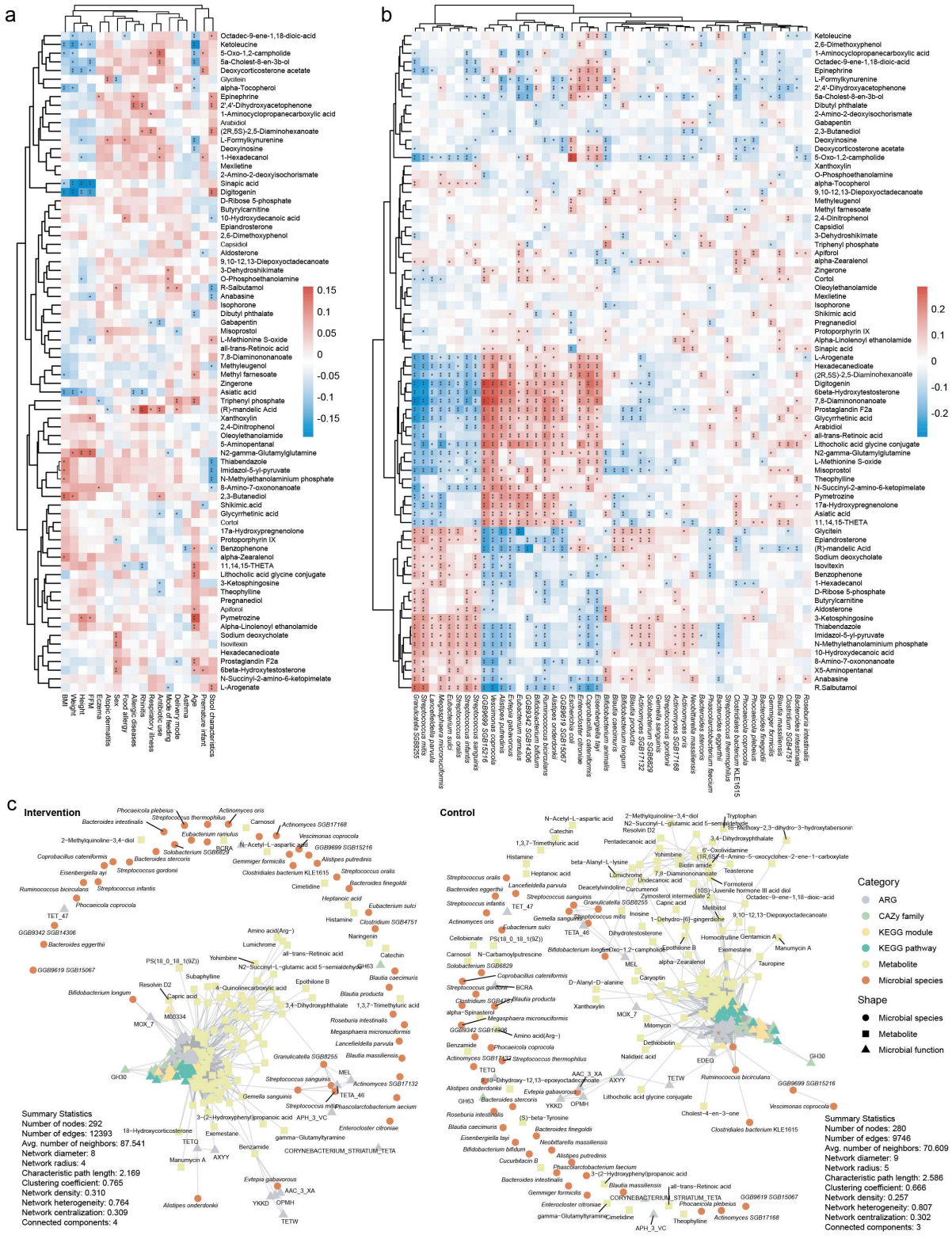


Figure 5

Multi-omics association patterns and co-occurrence networks linking microbes, metabolites, and clinical readouts in preschool children receiving Probio-M8 formula. (a) Heatmap of Spearman rank correlations between host phenotypes and differentially abundant fecal metabolites. Columns represent clinical variables, growth and body composition measures (height, weight, fat-free mass), gastrointestinal and respiratory outcomes, and antibiotic use; rows correspond to metabolites

significantly differing between intervention and control groups. **(b)** Heatmap of Spearman rank correlations between intervention-associated gut microbial species and differentially abundant fecal metabolites. Rows correspond to microbial species; columns refer to metabolites. In the heatmaps, color denotes the correlation coefficient (red, positive; blue, negative; *P < 0.05, **P< 0.01). **(c)** Integrated multi-omics co-occurrence networks for the intervention and control groups, constructed from significant Spearman correlations among differential gut species, metabolites, and functional features including antibiotic resistance gene (ARG), carbohydrate-active enzyme (CAZy) family, Kyoto Encyclopedia of Genes and Genomes (KEGG) module and pathway, metabolite, and microbial species. Nodes represent biological entities, colored by data type and shaped by category. Edges reflect significant correlations meeting thresholds for effect size and P value (r > 0.4, P < 0.01), with line thickness proportional to the absolute correlation coefficient. Summary network metrics are reported beneath each network.

Supplementary Files

This is a list of supplementary files associated with this preprint. Click to download.

- FigureS1.png
- FigureS2ZM.png
- FigureS3ZM.png
- FigureS4ZM.png